Journal of Asian Earth Sciences 42 (2011) 986–1007

Contents lists available at ScienceDirect

Journal of Asian Earth Sciences

journal homepage: www.elsevier.com/locate/jseaes

Late Devonian–Early Permian A-type granites in the southern Altay Range, Northwest China: Petrogenesis and implications for tectonic setting of "A_2-type" granites

Xiaoming Shen [a,b], Haixiang Zhang [a,*], Qiang Wang [a], Derek A. Wyman [c], Yueheng Yang [d]

[a] Key Laboratory of Isotope Geochronology and Geochemistry, Guangzhou Institute of Geochemistry, Chinese Academy of Sciences, Guangzhou 510640, China
[b] Graduate University of Chinese Academy of Science, Beijing 100049, China
[c] School of Geosciences, Division of Geology and Geophysics, The University of Sydney, NSW 2006, Australia
[d] Institute of Geology and Geophysics, Chinese Academy of Sciences, Beijing 100029, China

ARTICLE INFO

Article history:
Available online 31 October 2010

Keywords:
A-type granite
Ridge subduction
Post-collision
Altay
Central Asian Orogenic Belt

ABSTRACT

The Altay Range is an important part of the Central Asian Orogenic Belt (CAOB) that contains A-type granites that have been attributed to a post-collisional setting during the Late Carboniferous–Permian. However, our new LA-ICP-MS zircon U–Pb age data demonstrates that there were two episodes of A-type granite magmatism in the southern Altay Range. A Late Carboniferous to Early Permian (308–291 Ma) suite does occur in the vicinity of Qiakuerte but a distinct Late Devonian (382–367 Ma) suite is present in the Kouan area. The early Kouan A-type granites are mainly composed of alkali-feldspar granites, which are approximately synchronous with adakites, boninites, high-Ti basalts, picrites, ophiolitic rocks, and high temperature-low pressure metamorphic rocks, whereas the late Qiakuerte A-type granites mainly consist of arfvedsonite and aegirine-bearing granites, which are approximately coeval with some mafic–ultramafic rocks in the southern Altay Range. A-type granites are commonly classified as A_1 and A_2 sub-types, which are considered to be generated in anorogenic (rift or plume-related) or post-collisional settings, respectively. Both suites of the southern Altay Range are geochemically similar to typical A_2-type granites, e.g., high $K_2O + Na_2O$, FeO/MgO, and Ga/Al, and Y/Nb values, and low CaO, Ba, Sr, and Eu contents. The Kouan A-type granites have relatively low $(La/Yb)_N$ (2.7–5.9), high $\varepsilon_{Nd}(t)$ (+6.7 to +7.7) and Nb/La (0.59–1.67), and variable $\varepsilon_{Hf}(t)$ (+5.0 to +14.1) values, whereas the Qiakuerte A-type granites have comparatively high $(La/Yb)_N$ (4.2–9.2), low $\varepsilon_{Nd}(t)$ (+5.3 to +6.0) and Nb/La (0.33–0.74), and variable $\varepsilon_{Hf}(t)$ (+10.0 to +18.7) values. The early Kouan A-type granites may have been generated by partial melting of a mafic source containing more depleted mantle-derived components than the late Qiakuerte A-type granites. We suggest that the Late Carboniferous to Early Permian Qiakuerte granites were formed in a post-collisional extensional setting, as is typical of A_2-type granites. However, the Late Devonian Kouan A-type granites were more plausibly generated in an extensional setting as a result of slab window caused by a ridge subduction. In this case, the upwelling of asthenosphere through the slab window provided the source of parental magmas, or the heat for the generation of Devonian magmas. Therefore, our results suggest that A_2-type granites can also form in a ridge subduction-related extensional setting.

1. Introduction

A-type granites were first distinguished by Loiselle and Wones (1979) and have been extensively studied due to their unusual origins and tectonic settings (Collins et al., 1982; Whalen et al., 1987; Creaser et al., 1991; Eby, 1992; Frost and Frost, 1997; King et al., 1997; Bonin, 2007; Dall'Agnol and de Oliveira, 2007). They were originally considered to have been generated in an "anorogenic" setting (Loiselle and Wones, 1979). However, Eby (1992) subdivided A-type granites into two sub-types and suggested that they may have different origins and tectonic settings. The A_1-type granites represent differentiates of magmas derived from OIB-like sources but emplace in continental rifts or during intraplate magmatism (Eby, 1992). The A_2-type granites are derived from partial melting of continental crust or underplated mafic crust that has been through a cycle of continent-continent collision or a subduction zone and were mainly formed in a post-collision extensional setting (Eby, 1992). This concept was widely accepted and applied in the study of A-type granites (Han et al., 1997; Wu et al., 2002; Li et al., 2007; Zhang et al., 2007a; Zhao et al., 2008; Zhou et al., 2008).

* Corresponding author.
E-mail address: zhanghx@gig.ac.cn (H. Zhang).

1367-9120/$ - see front matter © 2010 Elsevier Ltd. All rights reserved.
doi:10.1016/j.jseaes.2010.10.004

The Central Asian Orogenic Belt (CAOB) (also named the Altaid Collage or the Altaids), one of the world's largest accretionary orogens, was mainly formed by subduction and accretion of juvenile material from the Neoproterozoic through to the Paleozoic (Sengör et al., 1993; Jahn et al., 2000, 2004; Xiao et al., 2009). Large volumes of Paleozoic magmatic rocks occur in the CAOB, including A-type granites (Liu and Yuan, 1996; Zhao et al., 1996; Han et al., 1997; Chen and Jahn, 2002, 2004; Liu, 2002; Wu et al., 2002; Liu et al., 2005; Su et al., 2006, 2008; Konopelko et al., 2007; Guo et al., 2008; Mao et al., 2008b; Zhou et al., 2008; Tang et al., 2010a). However, all reported A-type granites were generated in the Carboniferous to Cretaceous (338–106 Ma). The southern Altay Range, which is a part of the CAOB, is also characterized by widespread occurrence of Paleozoic magmatic rocks, most of which are Late Carboniferous–Early Permian A-type granites (Liu and Yuan, 1996; Zhao et al., 1996; Han et al., 1997; Chen and Jahn, 2004; Mao et al., 2008b; Su et al., 2008). These granites are geochemically similar to A_2-type granites and were considered to have been generated in a post-collisional setting.

We recently investigated several A-type granite plutons in the southern margin of the Altay Range, northern Xinjiang (Northwest China). Our data suggest that there are not only Late Carboniferous–Early Permian A-type granites, but also Late Devonian A-type granites in this district and both exhibit A_2-type geochemical characteristics. In this study, we report their zircon U–Pb ages, major and trace element compositions and Nd–Hf isotope characteristics. We suggest that the Late Carboniferous–Early Permian A_2-type granites were formed in a post-collisional setting, whereas the Late Devonian A_2-type granites were generated in a ridge subduction-related extensional setting.

2. Geological setting

The Altay Range is geographically located along the border regions between Russia and Kazakhstan to the west and Western China and Western Mongolia to the east. Tectonically, it lies in the central part of the CAOB, along the northern margin of the Kazakstan-Junggar Plate (Fig. 1a). The southern Altay Range of the northern Xinjiang Province (Northwest China) is located to the northeast of the Junggar Basin. From north to south, it is tectonically divided into the Altay arc, Dulate arc, and Yemaquan arc, which are separated by the Ertix and Zhaheba-Armantai fault zones (Xiao et al., 2008, 2009) (Fig. 1b).

There are three ophiolite zones in the southern Altay Range that, from north to south, include the Qiaoxiahala-Qinghe, Zhaheba-Armantai and Kalamaili ophiolites. These occur along the Ertix, Zhaheba-Armantai and Kalamaili fault zones, respectively (Fig. 1b). Tholeiites from the Qinghe ophiolite have a zircon SHRIMP U–Pb age of 352 ± 4 Ma (Wu et al., 2006a), which is the youngest among all the ophiolites in the southern Altay. Plagiogranites from the Kuerti ophiolite in the northern part of the Qiaoxiahala-Qinghe ophiolites have a zircon SHRIMP U–Pb age of 372 ± 19 Ma (Zhang et al., 2003a), which is slightly older than or approximately coeval, within error ranges, with the Qinghe ophiolites. The Zhaheba-Armantai ophiolite has zircon SHRIMP U–Pb ages ranging from 406 to 503 Ma (Jian et al., 2003; Xiao et al., 2009). Gabbros and anorthosite from the Zhaheba ophiolite have zircon SHRIMP U–Pb ages of 406–489 Ma, which is consistent with the presence of Devonian–Ordovician radiolarian cherts (Li et al., 1990; Xiao and Tang, 1991; Xiao et al., 1992; He et al., 2001). Plagiogranites of the Armantai ophiolite have a zircon SHRIMP U–Pb age of 503 ± 7 Ma (Xiao et al., 2009). The Late Cambrian–Ordovician Zhaheba-Armantai ophiolite has been interpreted as ancient oceanic crust of the Junggar Ocean (Deng and Wang, 1995; Jian et al., 2003; Xiao et al., 2009). Plagiogranites of the Kalamaili ophiolites have a zircon SHRIMP U–Pb age of 373 ± 10 Ma (Tang et al., 2007a). The ophiolite age data indicate that formation of oceanic basins in the region occurred in the Paleozoic. These oceanic basins may have closed in the Carboniferous, given the presence of continental deposits that abruptly overlie early Paleozoic marine facies deposits (Zhou et al., 2006; Charvet et al., 2007; Zhang et al., 2009).

The rocks outcropping in the southern Altay Range consist of Ordovician–Silurian gneisses and schists, a Devonian to Early Carboniferous marine volcanic-sedimentary rock sequence, a Late Carboniferous to Permian continental volcanic-sedimentary rock sequence, Mesozoic coal-bearing sedimentary rocks and Cenozoic sediments (Fig. 1b) (Zhou et al., 2006; Zhang et al., 2008a) (Fig. 1b). Early Paleozoic rocks mainly occur to the north of the southern Altay Range and Late Paleozoic to the south (Fig. 1b). Paleozoic rock types of the southern Altay Range are summarised in Table 1.

Late Paleozoic volcanic rocks in the southern Altay Range have recently been studied in some detail (Zhang et al., 2003b, 2005, 2008a, 2009; Niu et al., 2006). Boninites were found in the Middle Devonian Beitashan Formation in the Shaerbulake area, ca. 20 km southwest of Fuyun City (Zhang et al., 2003b; Niu et al., 2006). Picrites were also discovered in the lower part of the Beitashan Formation (Zhang et al., 2008a). In addition, high-Ti basalts have been identified in Devonian strata of the Shaerbulake and Kuerti areas (Niu et al., 2006). All volcanic rocks from the Devonian Formations in the southern Altay Range are considered to have been generated in a Devonian island-arc setting (Xiao et al., 2008; Zhang et al., 2009). Volcanic rocks of the Late Carboniferous Batamayineishan Formation, occurring to the south of the Dulate arc and locally with minor interbedded carbonaceous shale, are considered to have mainly formed in either a post-collisional or arc setting (Long et al., 2006; Xiao et al., 2008; Wu et al., 2009; Zhang et al., 2009).

In addition to the Late Paleozoic volcanic rocks, the southern Altay range also contains voluminous Paleozoic granitoids (Fig. 1b). In the Altay arc (Fig. 1b), the granitoids mainly consist of biotite granites, two-mica granites, and granodiorites. Most of the granitoids are metaluminous or weakly peraluminous and calc-alkaline (Chen and Jahn, 2002; Wang et al., 2006, 2009; Yuan et al., 2007). Zircon U–Pb age data indicate that these granitoids were mostly emplaced between 360 Ma and 460 Ma (Wang et al., 2006, 2009; Yuan et al., 2007; Sun et al., 2008, 2009). However, in the Dulate and Yemaquan arc, the granitoids, which mainly consist of biotite granites, diorites, granodiorites, alkali granites, and alkali-feldspar granite, were mostly emplaced at 270–320 Ma (Liu and Yuan, 1996; Han et al., 1997, 2006a; Tang et al., 2007b; Mao et al., 2008b; Su et al., 2008) with the exception of several 376–393 Ma adakitic plutons (granodiorite, monzodiorite, and quartz diorite porphyries) (Yang et al., 2005a; Wan and Zhang, 2006; Zhang et al., 2006; Xiang et al., 2009).

A number of alkali granite, alkali-feldspar granite, monzogranite, and biotite granite intrusions in the Dulate and Yemaquan arc are geochemically similar to A-type granites (Liu and Yuan, 1996; Zhao et al., 1996; Han et al., 1997; Windley et al., 2002). In the southern part of the Altay Range, A-type granite plutons occur along the Kalamaili fault zone and have zircon U–Pb ages of 306–284 Ma (Tang et al., 2007b; Mao et al., 2008b; Su et al., 2008). In the central part of the range, A-type granite plutons occur close to the Zhaheba-Armantai ophiolite belt (Han et al., 1997; Chen and Jahn, 2004). Previous Rb–Sr whole-rock or biotite-whole-rock isochron age data suggested that these A-type granite plutons were emplaced at about 300–270 Ma (Han et al., 1997; Chen and Jahn, 2004). These A-type granitoids in the southern Altay Range are temporally associated with Cu–Ni bearing mafic and ultramafic plutons (Kalatongke) having a SHRIMP zircon U–Pb age of 287 ± 5 Ma (Han et al., 2004) and Re–Os sulfide mineral isochron age of 283–305 Ma (Han et al., 2006b; Zhang et al., 2008b).

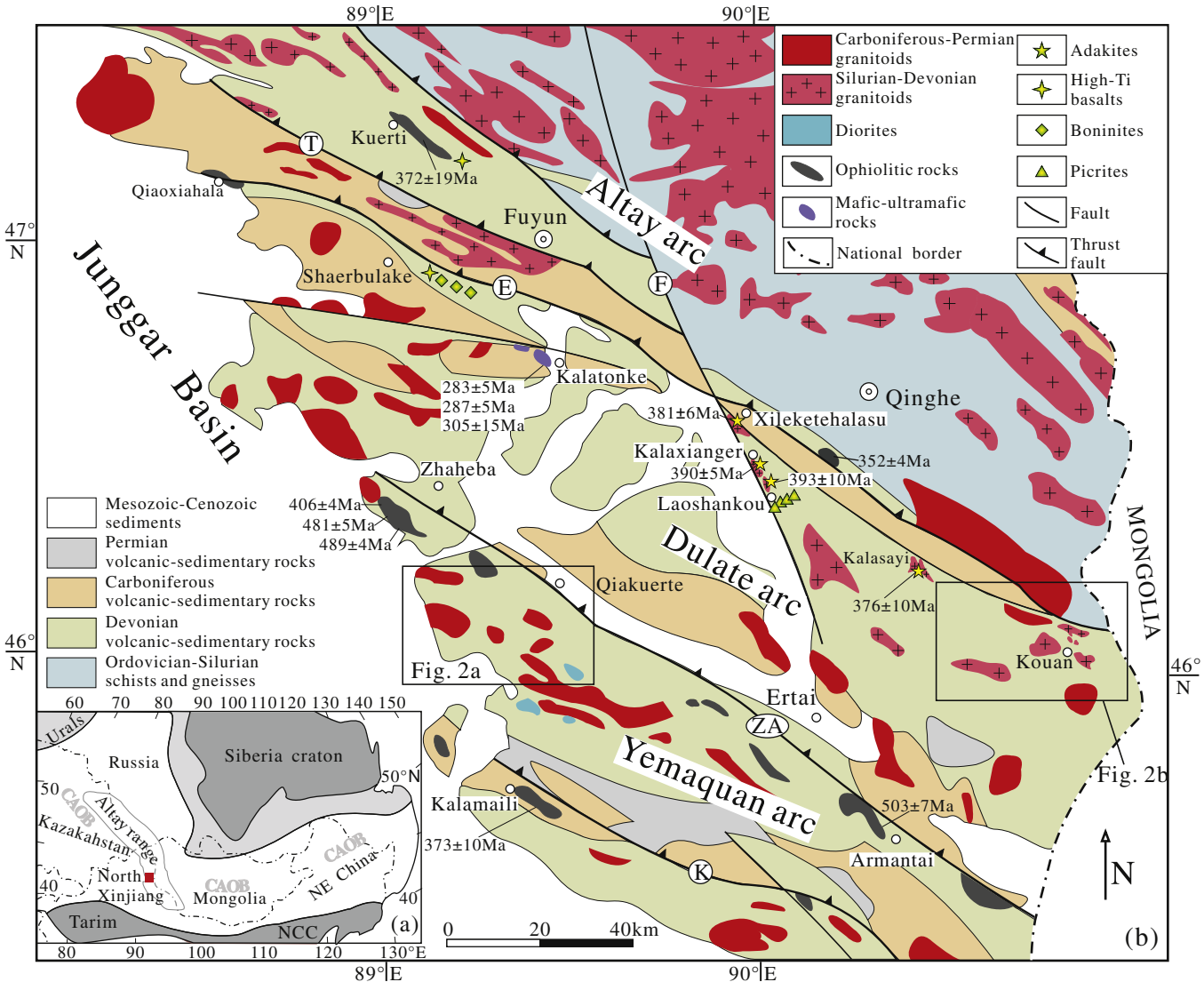

Fig. 1. (a) Location of the study area in the Central Asian Orogenic Belt (modified after Sengör et al., 1993; Jahn et al., 2000). (b) Geological map of the southern Altay Range (modified from Windley et al., 2002; Wang et al., 2009). Major faults: E—Ertix thrust; F—Fuyun fault; ZA—Zhaheba-Armantai thrust; K—Kalamaili thrust. Ages shown for rocks are from Zhang et al. (2006), Xiao et al. (2008) and Xiang et al. (2009) and references therein.

Table 1
The types of the Paleozoic rocks in the southern Altay Range.

Period	Formation	Rock types
Permian	Harjiawu	Basic-acid volcanic rocks, welded tuff, tuffaceous breccia, sedimentary tuff, clastic sedimentary and coal-bearing sedimentary rocks
Late Carboniferous	Batamayineishan	Basalts and basaltic andesites, locally with minor interbedded tuff, siltstone and carbonaceous shale
Early Carboniferous	Nanmingshui	A succession of volcanic–sedimentary rocks: basalt, andesite, tuff, chert, tuffaceous slate, sandstone, black shale, sedimentary-volcanic breccia, carbonaceous slate and limestone
Late Devonian	Jiangzierkuduke	Pyroclastic rocks (dominated by tuff) intercalated with sandstone, basaltic andesite, andesite and dacite
Middle Devonian	Yundukala	A suite of shallow marine fine clastic rocks interbedded with basic rocks and intermediate rocks
	Beitashan	Basalt, basaltic tuff, basaltic breccia, picrite, sedimentary tuff, chert, siltstone and sandstone
Early Devonian	Tuoranggekuduke	Basic-acid volcanic rocks, pyroclastic rocks, siltstone, tuff and tuffaceous sandstone
Ordovician-Silurian	Habahe	Sandstone, siltstone, mudstone, and slate

Samples from five representative granite plutons (Saertielieke, Jierdekala, West-Kouan, East-Kouan and North-Kouan) in the southern Altay Range were collected for this study (Figs. 1b and 2). The Saertielieke and Jierdekala plutons are located to the southwest of Qiakuerte town and intruded into the Late Devonian Jiangzierkuduke Formation (Fig. 2a). The two plutons are massive and undeformed and exhibit massive structure (Fig. 3a). The West-Kouan, East-Kouan and North-Kouan plutons are located

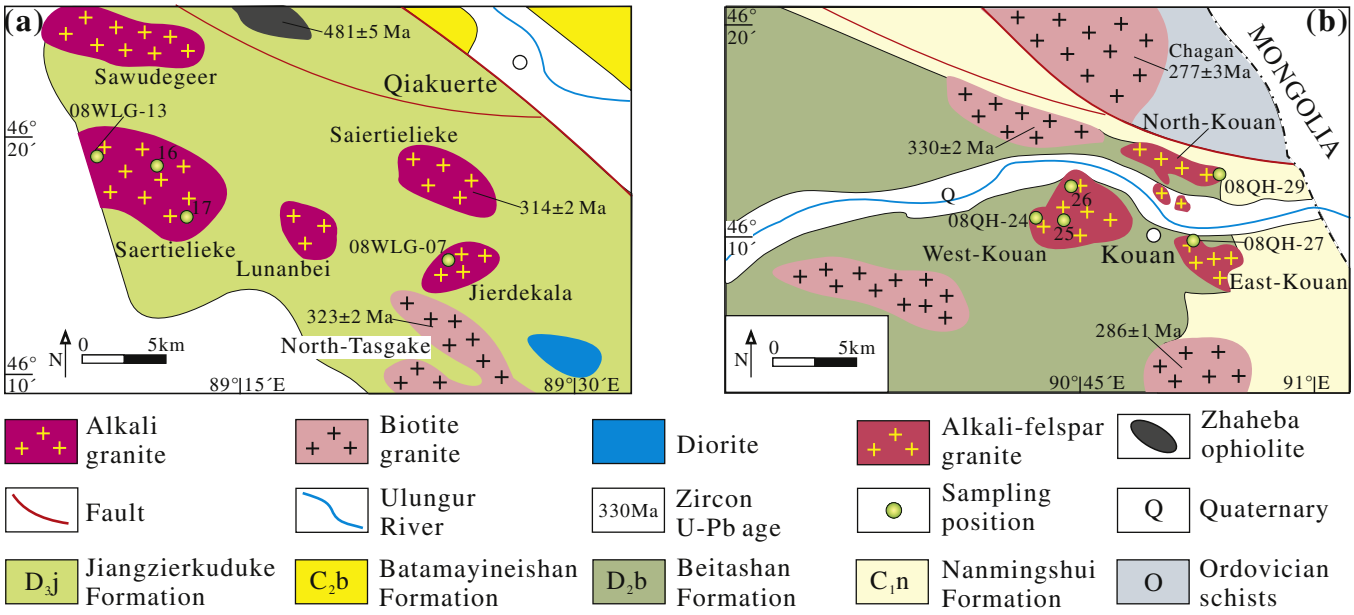

Fig. 2. Geological maps of (a) Qiakuerte and (b) Kouan areas in the southern Altay Range. Zircon U–Pb ages shown for rocks are from Liu and Yuan (1996), Jian et al. (2003), Tong et al. (2006), and our unpublished data.

around the town of Kouan. They intrude the Middle Devonian Beitashan Formation and are slightly deformed (Fig. 3c).

3. Petrography

The alkali granite Saertielieke and Jierdekala plutons are pink at fresh outcrops (Fig. 3a) and have coarse to medium grained texture. They consist of arfvedsonite (3–5%), aegirine (1–5%), perthite (40–60%), albite (2–3%), quartz (20–50%) and minor accessory minerals (e.g., zircon, apatite and magnetite) (Fig. 3b). Arfvedsonite and aegirine occur as anhedral grains coexisting with subhedral feldspar and anhedral quartz. Some acicular arfvedsonite crystals and irregular aegirine crystals are enclosed in the feldspar crystals, and arfvedsonite granules may be rimmed or occasionally replaced by aegirine. Some quartz and feldspar exhibit micrographic textures.

The West-Kouan, East-Kouan and North-Kouan plutons mainly consist of alkali-feldspar granites. They are pink or grey at fresh outcrops and have coarse to medium grained texture. They are composed of biotite (1–5%), perthite (30–40%), K-feldspar (10–20%), quartz (30–50%) and accessory minerals (e.g., zircon, apatite and magnetite), and lack alkali mafic minerals (e.g., arfvedsonite and aegirine). Quartz and feldspar also exhibit micrographic textures (Fig. 3d).

4. Analytical methods

4.1. Zircon U–Pb geochronology

Two samples (08WLG-16 and 08WLG-07) from the Saertielieke and Jierdekala plutons in the Qiakuerte area and two samples (08QH-25 and 08QH-27) from the West-Kouan and East-Kouan plutons in the Kouan area were analyzed in this study. Zircon grains were separated using conventional heavy liquid and magnetic techniques, followed by handpicking. The representative grains were mounted in epoxy, polished, and photographed in transmitted and reflected light, followed by cathodeluminescence (CL) and backscatter electron (BSE) imaging in order to identify the structure of the zircon grains. CL and BSE imaging was carried out using a JXA-8100 Electron Probe Microanalyzer with a Mono CL3 Cathode luminescence System for high resolution imaging and spectroscopy at the Key Laboratory of Isotope Geochronology and Geochemistry (KLIGG), Guangzhou Institute of Geochemistry, Chinese Academy of Sciences (GIGCAS). U–Pb dating was conducted by LA-ICP-MS at the State Key Laboratory of Geological Processes and Mineral Resources, China University of Geosciences, Wuhan. Laser sampling was performed using an excimer laser-ablation system (GeoLas 2005). An Agilent 7500a ICP-MS instrument was used to acquire ion-signal intensities. Helium was used as a carrier gas. Argon was used as the make-up gas and mixed with the carrier gas via a T-connector before entering the ICP. Because high-purity argon and helium (>99.999%) were used, both the ^{204}Pb and ^{202}Hg intensities of the gas blank were always lower than 50 c.p.s. at a sensitivity of 1 × 106 c.p.s. Spot sizes of 32 μm with a laser repetition rate of 8 Hz at 70 mJ were used. Detailed operating conditions for the laser and the ICP-MS instrument have been given by Liu et al. (2008). Each analysis incorporated a background acquisition of ~20–30 s (gas blank) followed by 50 s data acquisition from the sample. Details of the procedures for zircon analysis using LA-ICP-MS are described by Liu et al. (2010). Concordia diagrams and weighted mean calculations were made using Isoplot/Ex_ver3 (Ludwig, 2003).

4.2. Major and trace element analyses

Representative samples were collected from Saertielieke, Jierdekala, West-Kouan, East-Kouan and North-Kouan plutons for major and trace element analysis. Selected relatively fresh rocks were first split into small chips and ultrasonically cleaned in distilled water, then powdered after drying and handpicking to remove visible alteration. Major element compositions were obtained by X-ray fluorescence spectrometry (XRF) on fused glass beads using a Rigaku 100e spectrometer at the KLIGG, GIGCAS. Details of the XRF procedures are described by Li et al. (2005). Trace elements, including rare earth elements (REE), were determined using a Perkin–Elmer ELAN 6000 inductively-coupled plasma source mass spectrometer (ICP-MS) at GIGCAS, following the procedures described by Li et al. (2002). The powdered samples (50 mg) were

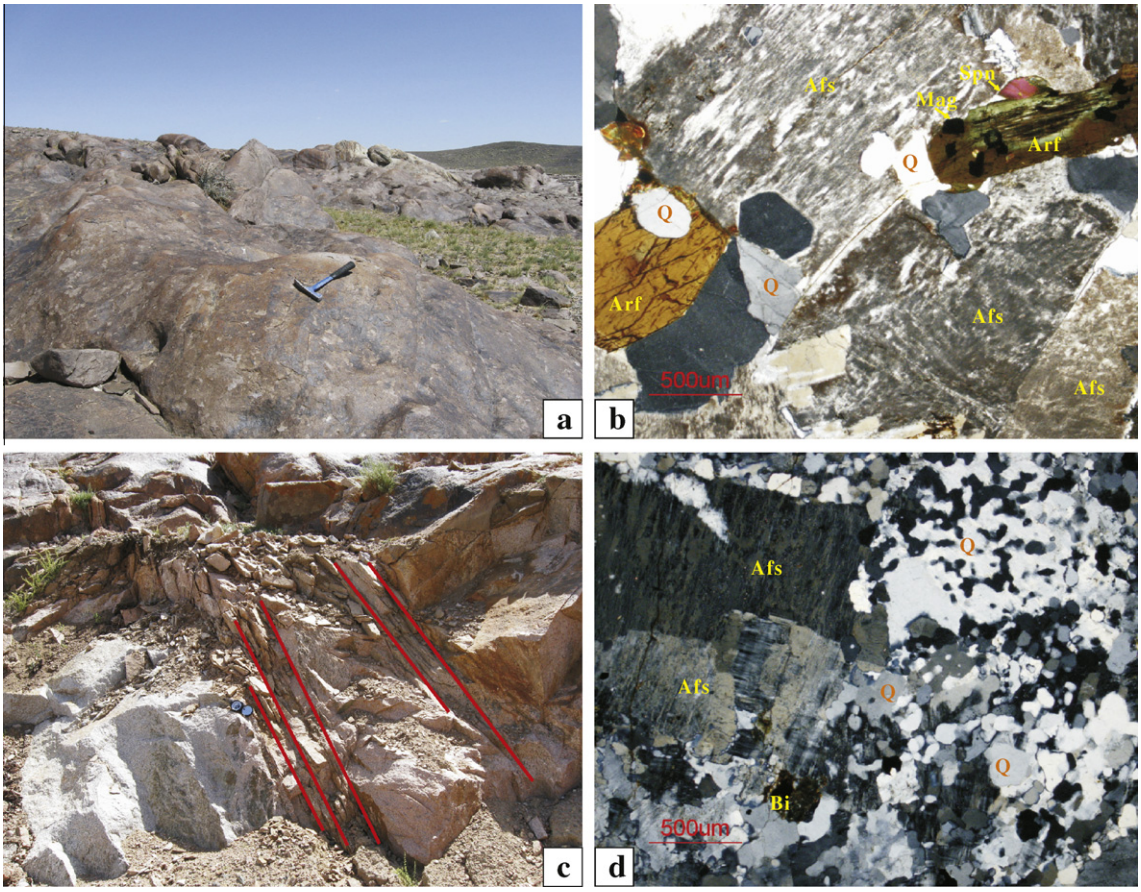

Fig. 3. Field outcrops of (a) the Jierdekala pluton and (c) West-Kouan pluton. Petrographic characteristics of the (b) Jierdekala alkali granite (Sample 08WLG-07) and (d) West-Kouan alkali-feldspar granite (08QH-24). Arf: arfvedsonite. Afs: alkali feldspar. Pl: Plagioclase. Q: quartz. Mag: magnetite. Spn: sphene.

dissolved in screw-top Teflon beakers using an HF + HNO_3 mixture for 7 days at ~100 °C. An internal standard solution containing the single element Rh was used to monitor drift in mass response during counting. USGS standard BCR-1 was used to calibrate the elemental concentrations of the measured samples. Precision for REE and other incompatible elements is estimated to be better than 5% from the international USGS reference samples BIR-1 and laboratory standard (ROA-1). In-run analytical precision for Nd is less than 2.5% RSD (relative standard deviation). The Sm/Nd ratios measured by ICP-MS are within 2% uncertainty, and the $\varepsilon_{Nd}(t)$ values of the samples using these Sm/Nd ratios result in uncertainties of less than 0.25ε unit, which are negligible for petrogenetic discussion.

4.3. Whole-rock Nd isotope analyses

Neodymium isotopic analyses were carried out using a Micromass Isoprobe multi-collector-inductively-coupled plasma mass spectrometry (MC-ICPMS) at the KLIGG, GIGCAS, using the analytical procedure described by Liang et al. (2003) and Li et al. (2006). Nd fractions were separated by passing through cation columns followed by HDEHP columns. Analyses of standard BHVO-2 during the period of analyses gave $^{143}Nd/^{144}Nd = 0.512976 \pm 9$ (2σ). Measured $^{143}Nd/^{144}Nd$ ratios were normalized to $^{146}Nd/^{144}Nd = 0.7219$.

4.4. Zircon Hf isotope analysis

In situ zircon Hf isotopic analysis was carried out on a Neptune multi-collector ICPMS equipped with a Geo-193 laser-ablation system (LA-MC-ICPMS) at the Institute of Geology and Geophysics, Chinese Academy of Sciences in Beijing, China. Spot sizes of 60 μm with a laser repetition rate of 10 Hz at 100 mJ were used. The detailed analytical technique and data correction procedure are described in Wu et al. (2006b). Zircon 91500 was used as the reference standard with a recommended $^{176}Hf/^{177}Hf$ ratio of 0.282306 (Woodhead et al., 2004). The chondritic values of $^{176}Hf/^{177}Hf$ (0.282772) and $^{176}Lu/^{177}Hf$ (0.0332) reported by Blichert-Toft and Albarède (1997) were used for the calculation of ε_{Hf} values. The ^{176}Lu decay constant of 1.865×10^{-11} year^{-1} (Scherer et al., 2001) was used to calculate initial $^{176}Lu/^{177}Hf$ ratios. The depleted mantle Hf model ages (T_{DM}) were calculated using the measured $^{176}Lu/^{177}Hf$ ratios of zircon based on the assumption that the depleted mantle reservoir had a linear isotopic growth from $^{176}Hf/^{177}Hf = 0.279718$ at 4.55 Ga to 0.283250 at present, with $^{176}Lu/^{177}Hf = 0.0384$ (Griffin et al., 2000).

5. Results

5.1. Zircon U–Pb geochronology

Zircon grains from the Saertielieke and Jierdekala granites (Qiakuerte plutons) and the West-Kouan pluton are light-yellow and transparent to semi-transparent, and occur as euhedral stubby prismatic crystals with lengths of 100–150 μm and length/width ratios of 1.0–2.0 (Fig. 4). CL and BSE images clearly display oscillatory zoning in most crystals and the presence of old cores in some zircons. The results of LA-ICP-MS zircon analyses are listed in Table 2 and illustrated on a concordia plot in Fig. 4.

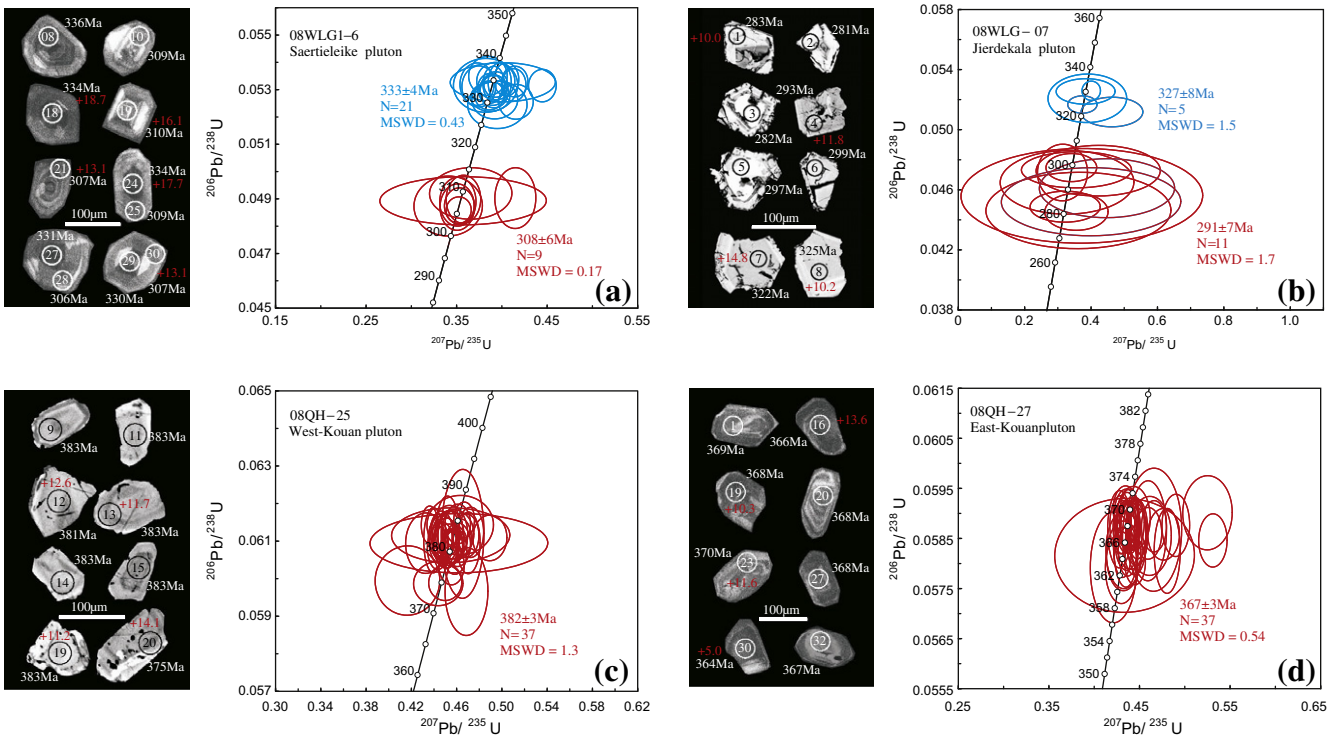

Fig. 4. Representative cathodeluminescence (CL) (a and d) or backscatter electron (BSE) (b and c) images and LA-ICPMS U–Pb concordant diagrams for zircons from the Saertielieke, Jierdekala, West-Kouan and East-Kouan granites.

Thirty spot analyses of zircons from Saertielieke granite sample 08WLG-16 yielded two groups of nearly concordant ages: the first group of ages from zircon cores have $^{206}Pb/^{238}U$ ages from 330 to 336 Ma and give a weighted mean of 333 ± 4 Ma (2σ); the second group of ages from zircon rims or well-crystallized zircon granules have $^{206}Pb/^{238}U$ ages from 306 to 310 Ma and give a weighted mean of 308 ± 6 Ma (2σ) (Table 2 and Fig. 4a). Thus, we suggest that 308 ± 6 Ma and 333 ± 4 Ma represent the ages of crystallization of the Saertielieke granite and the source material of the zircons, respectively. Eleven spot analyses of zircons from sample 08WLG-07 of the Jierdekala granite yield a single $^{206}Pb/^{238}U$ age population of 281–299 Ma, with a weighted mean of 291 ± 7 Ma (2σ) (Table 2 and Fig. 4b); this is the best estimate for their crystallization age. In addition, five zircons from sample 08WLG-07 also give a single $^{206}Pb/^{238}U$ age population of 322–331 Ma, with a weighted mean of 327 ± 8 Ma (2σ), which is consistent with the inherited zircon age (333 ± 4 Ma) of the Saertielieke granites.

Thirty-seven spot analyses of zircons from sample 08QH-25 of the West-Kouan granites yield a single $^{206}Pb/^{238}U$ age population of 385–374 Ma, with a weighted mean of 382 ± 3 Ma (2σ) (Table 2 and Fig. 4c); this is the best estimate for their crystallization age. Thirty-seven spot analyses of zircons from sample 08QH-27 of the East-Kouan granites yield a single $^{206}Pb/^{238}U$ age population of 370–363 Ma, with a weighted mean of 367 ± 3 Ma (2σ) (Table 2 and Fig. 4d); this is the best estimate for their crystallization age.

5.2. Major and trace element compositions

The samples from the West-Kouan, East-Kouan, and North-Kouan granites have high SiO_2 (69.4–76.9 wt%), K_2O (4.80–5.53 wt%) and $Na_2O + K_2O$ (8.97–10.3 wt%) contents, but low Na_2O/K_2O ratios (0.79–0.91) (Table 3; Figs. 5a and b). All the granite samples plot in the high-K calc-alkaline field in the K_2O versus SiO_2 diagram (Fig. 5a). They have Al_2O_3 contents ranging from 12.4 and 15.1 wt% and exhibit weakly metaluminous characteristics on a plot of A/NK (molar $Al_2O_3/Na_2O + K_2O$) versus A/CNK (molar $Al_2O_3/CaO + Na_2O + K_2O$) (Fig. 5c). They have low MgO (0.02–0.33 wt%), CaO (0.27–1.0 wt%), and P_2O_5 (<0.07 wt%) and high $Fe^{\#}$ ($FeO^{tot}/(FeO^{tot} + MgO)$ = 0.87–0.98) values (Table 3; Fig. 5d). The Kouan granites have similar chondrite-normalized REE patterns that are enriched in light rare earth elements (LREE) ($(La/Yb)_N$ = 2.67–5.87), display pronounced negative Eu anomalies (average Eu/Eu^* = 0.11) (Fig. 6a), and have nearly flat heavy rare earth elements (HREE) ($(Tb/Yb)_N$ = 0.89–1.27). On primitive-mantle normalized diagrams, they show prominent negative Ba, Sr, Eu, and Ti anomalies, and slightly negative or positive Nb anomalies (Fig. 6b).

The Saertielieke and Jierdekala granites in the Qiakuerte area also have high SiO_2 (73.9–77.4 wt%) and $Na_2O + K_2O$ (8.1–10.0 wt%) contents, but lower K_2O (4.10–4.90 wt%) and higher Na_2O/K_2O ratios (0.95–1.04) (Table 3; Fig. 5a and b) than those of the Kouan granites. All the granite samples also plot in the high-K calc-alkaline field on a K_2O versus SiO_2 diagram (Fig. 5a). They mainly display peralkaline characteristics on a plot of A/NK versus A/CNK (Fig. 5c) and also show high $Fe^{\#}$ values (Fig. 5d). The Qiakuerte granites also have flat HREE patterns, but are more enriched in LREE ($(La/Yb)_N$ = 4.23–9.17) than those from the Kouan area (Fig. 6a). Although their primitive-mantle normalized diagrams also show pronounced negative Ba, Sr, Eu, Ti, and slightly negative Nb anomalies (Fig. 6b), they have lower Ba, Sr, Nb and Ta but higher Zr, Hf and Ti contents than those of the Kouan granites.

Both the Kouan and Qiakuerte granites plot in the field of within-plate granites (Fig. 7a). They have high Zr, Nb and 10,000 × Ga/Al values, indicating that they are geochemically similar to A-type granites (Fig. 7b and c).

Table 2
Zircon LA-ICP-MS U–Pb data of the A-type granites in the southern Altay Range.

Spot	Pb_{rad}	^{238}U (ppm)	^{232}Th (ppm)	Th/U	Isotopic ratios						Apparent age (Ma)					
					$^{207}Pb/^{206}Pb$	1σ	$^{207}Pb/^{235}U$	1σ	$^{206}Pb/^{238}U$	1σ	$^{207}Pb/^{206}Pb$	1σ	$^{207}Pb/^{235}U$	1σ	$^{206}Pb/^{238}U$	1σ
08WLG-16 (Saertielieke pluton)																
1	47.4	611.3	1234.7	2.02	0.05186	0.00164	0.35086	0.01259	0.04874	0.00056	279	61	305	9	307	3
2	14.5	242.6	231.2	0.95	0.05212	0.00198	0.35133	0.01332	0.04894	0.00059	291	65	306	10	308	4
3	13.3	210.3	182.9	0.87	0.05085	0.00166	0.37442	0.01246	0.05315	0.00049	234	60	323	9	334	3
4	26.5	394.8	388.1	0.98	0.05311	0.00104	0.39068	0.00781	0.05325	0.00042	334	31	335	6	334	3
5	19.0	292.2	311.0	1.06	0.05714	0.00172	0.41545	0.01254	0.05259	0.00042	497	53	353	9	330	3
6	19.2	308.1	245.3	0.80	0.05348	0.00191	0.39308	0.01377	0.05334	0.00045	349	64	337	10	335	3
7	52.3	684.0	1054.2	1.54	0.05492	0.00127	0.40466	0.00911	0.05340	0.00040	409	37	345	7	335	2
8	40.0	556.9	672.5	1.21	0.05198	0.00182	0.38459	0.01392	0.05353	0.00047	285	67	330	10	336	3
9	25.2	356.2	454.2	1.28	0.05069	0.00167	0.37251	0.01238	0.05323	0.00051	227	59	322	9	334	3
10	21.6	346.5	375.6	1.08	0.06114	0.00203	0.41474	0.01491	0.04907	0.00073	644	52	352	11	309	4
11	24.3	359.2	420.5	1.17	0.05628	0.00117	0.41315	0.00889	0.05320	0.00039	463	35	351	6	334	2
12	30.1	373.1	560.3	1.50	0.05303	0.00516	0.40085	0.03830	0.05330	0.00047	330	202	342	28	335	3
13	16.6	255.6	243.1	0.95	0.05399	0.00234	0.39205	0.01668	0.05266	0.00046	371	100	336	12	331	3
14	18.3	290.1	246.0	0.85	0.05290	0.00127	0.38690	0.00903	0.05308	0.00036	324	41	332	7	333	2
15	23.9	326.0	460.1	1.41	0.05402	0.00108	0.39750	0.00820	0.05329	0.00047	372	31	340	6	335	3
16	15.2	235.0	220.1	0.94	0.05321	0.00128	0.39003	0.00974	0.05302	0.00037	338	44	334	7	333	2
17	29.1	404.7	560.7	1.39	0.05212	0.00333	0.38211	0.02339	0.05319	0.00065	291	118	329	17	334	4
18	35.5	511.7	676.0	1.32	0.05369	0.00449	0.36552	0.02985	0.04924	0.00062	358	163	316	22	310	4
19	21.3	336.5	271.0	0.81	0.05348	0.0014	0.39125	0.01028	0.05296	0.00039	349	46	335	8	333	2
20	13.3	207.0	190.2	0.92	0.05092	0.00408	0.34074	0.02504	0.04878	0.00072	237	140	298	19	307	4
21	63.5	579.0	920.9	1.59	0.05217	0.00846	0.35723	0.06062	0.04897	0.00058	293	328	310	45	308	4
22	39.3	519.2	765.5	1.47	0.06056	0.00144	0.44449	0.01009	0.05318	0.00039	624	36	373	7	334	2
23	26.4	395.6	549.6	1.39	0.05293	0.00202	0.35754	0.01262	0.04903	0.00058	326	59	310	9	309	4
24	19.1	271.3	337.4	1.24	0.05629	0.00130	0.41418	0.00952	0.05332	0.00037	464	39	352	7	335	2
25	34.6	486.3	566.0	1.16	0.05306	0.00194	0.38706	0.01409	0.05277	0.00035	331	71	332	10	331	2
26	21.3	340.3	296.5	0.87	0.05264	0.00141	0.35237	0.00915	0.04863	0.00032	313	47	307	7	306	2
27	19.2	302.3	230.1	0.76	0.05457	0.00305	0.39478	0.02168	0.05247	0.00057	395	129	338	16	330	3
28	22.0	354.2	335.2	0.95	0.05245	0.00159	0.35303	0.01079	0.04879	0.00043	305	54	307	8	307	3
29	28.0	419.5	438.8	1.05	0.05355	0.00118	0.39324	0.00855	0.05322	0.00031	352	39	337	6	334	2
30	31.5	388.1	776.5	2.00	0.05294	0.00145	0.38626	0.01077	0.05282	0.00035	326	51	332	8	332	2
08WLG-07 (Jierdekala pluton)																
1	120.8	911.1	2148.4	2.36	0.05125	0.01114	0.32206	0.06973	0.04495	0.00068	252	380	283	54	283	4
2	275.5	752.6	3057.7	4.06	0.05767	0.01044	0.35531	0.06284	0.04461	0.00081	517	359	309	47	281	5
3	866.7	1622.4	11201.7	6.90	0.05207	0.02512	0.36155	0.18328	0.04470	0.00167	288	863	313	137	282	10
4	235.2	476.5	895.3	1.88	0.04965	0.02090	0.32737	0.13257	0.04657	0.00139	179	650	288	101	293	9
5	79.6	1162.0	421.7	0.36	0.04779	0.00638	0.31345	0.04974	0.04722	0.00124	89	271	277	38	297	8
6	144.0	598.1	1123.1	1.88	0.04857	0.01694	0.35541	0.10909	0.04740	0.00079	127	490	309	82	299	5
7	107.2	751.6	449.4	0.60	0.06195	0.00792	0.46211	0.06136	0.05123	0.00065	672	273	386	43	322	4
8	79.9	452.9	1218.3	2.69	0.05125	0.00399	0.37391	0.02898	0.05173	0.00038	252	163	323	21	325	2
9	1099.2	1840.7	2389.1	1.30	0.04929	0.00662	0.34015	0.05022	0.04755	0.00061	162	278	297	38	299	4
10	1100.5	918.4	105.8	0.12	0.04849	0.01863	0.42061	0.12294	0.04733	0.00111	123	459	356	88	298	7
11	2438.6	399.1	88.5	0.22	0.04665	0.03581	0.37181	0.23953	0.04567	0.00208	31	959	321	177	288	13
12	1753.9	1211.6	5736.9	4.73	0.05080	0.00792	0.38273	0.05861	0.05261	0.00056	232	298	329	43	331	3
13	1664.4	398.3	531.0	1.33	0.04810	0.02638	0.39972	0.17780	0.04527	0.00149	104	703	341	129	285	9
14	2573.9	962.8	249.1	0.26	0.06652	0.0195	0.44722	0.13437	0.04618	0.00129	823	575	375	94	291	8
15	540.8	729.1	642.7	0.88	0.05135	0.01041	0.38863	0.07796	0.05214	0.00106	257	349	333	57	328	6
16	35.5	499.2	68.1	0.14	0.05494	0.00251	0.39993	0.01814	0.05265	0.00042	410	88	342	13	331	3
08QH-25 (West-Kouan pluton)																
1	252.6	2312.4	1787.3	0.77	0.0522	0.00583	0.46201	0.05171	0.06097	0.00052	294	239	386	36	382	3
2	150.5	2352.6	847.6	0.36	0.05137	0.00132	0.43261	0.01168	0.06097	0.00053	257	46	365	8	382	3
3	290.5	4023.0	4691.4	1.17	0.05390	0.00121	0.45387	0.01008	0.06101	0.00031	367	41	380	7	382	2
4	286.0	4218.8	470.1	0.11	0.05367	0.00175	0.44373	0.01436	0.05990	0.00039	357	62	373	10	375	2

5	322.4	4832.3	2366.2	0.49	0.05404	0.00140	0.45683	0.01209	0.06121	0.00043	373	47	382	8	383	3
6	326.7	5019.2	2144.6	0.43	0.05458	0.00072	0.45858	0.00691	0.06075	0.00040	395	22	383	5	380	2
7	166.5	2519.1	1280.3	0.51	0.05275	0.00068	0.44333	0.00610	0.06085	0.00038	318	20	373	4	381	2
8	336.4	5168.9	1881.3	0.36	0.05293	0.00073	0.44633	0.00696	0.06098	0.00037	326	24	375	5	382	2
9	293.8	4405.3	1990.2	0.45	0.05476	0.00075	0.46504	0.01248	0.06122	0.00113	403	30	388	9	383	7
10	271.6	4148.9	1156.6	0.28	0.05349	0.00102	0.45339	0.01073	0.06120	0.00051	350	38	380	7	383	3
11	381.6	3665.1	3416.5	0.93	0.05324	0.00396	0.45461	0.03441	0.06118	0.00048	339	159	381	24	383	3
12	232.1	3608.3	1384.4	0.38	0.05405	0.00057	0.45444	0.00497	0.06083	0.00031	373	16	380	3	381	2
13	163.6	2632.7	863.2	0.33	0.05337	0.00068	0.45197	0.00696	0.06127	0.00063	345	18	379	5	383	4
14	106.7	1693.5	547.0	0.32	0.05572	0.00083	0.47215	0.00761	0.06126	0.00044	441	23	393	5	383	3
15	244.3	3703.1	1669.3	0.45	0.05275	0.00075	0.44639	0.00684	0.06117	0.00043	318	22	375	5	383	3
16	132.3	2077.1	731.1	0.35	0.05534	0.00085	0.46820	0.00742	0.06117	0.00038	426	24	390	5	383	2
17	204.0	2761.6	1882.3	0.68	0.05438	0.00218	0.46310	0.01931	0.06145	0.00052	387	79	386	13	384	3
18	93.9	1409.9	530.3	0.38	0.05422	0.00085	0.46110	0.00736	0.06148	0.00035	380	26	385	5	385	2
19	368.2	5504.7	2463.2	0.45	0.05405	0.00073	0.45546	0.00632	0.06090	0.00030	373	22	381	4	381	2
20	266.8	4039.4	1853.3	0.46	0.05381	0.00093	0.45487	0.00762	0.06113	0.00046	363	24	381	5	383	3
21	111.4	1681.2	708.5	0.42	0.05027	0.00239	0.41651	0.01888	0.05998	0.00061	207	86	354	14	375	4
22	140.3	2182.2	822.0	0.38	0.05373	0.00069	0.45626	0.00582	0.06137	0.00030	360	20	382	4	384	2
23	182.4	2836.7	1119.4	0.39	0.05456	0.00095	0.45561	0.00743	0.06038	0.00034	394	26	381	5	378	2
24	125.9	1919.4	790.5	0.41	0.05480	0.00073	0.46666	0.00598	0.06159	0.00031	404	20	389	4	385	2
25	139.3	2212.0	715.7	0.32	0.05345	0.00092	0.45088	0.00725	0.06097	0.00044	348	23	378	5	382	3
26	301.8	4546.0	1982.1	0.44	0.05434	0.00067	0.45790	0.00574	0.06088	0.00028	385	20	383	4	381	2
27	182.2	2730.9	1353.6	0.50	0.05495	0.00068	0.46445	0.00569	0.06109	0.00034	410	18	387	4	382	2
28	239.7	3681.3	1380.3	0.37	0.05571	0.00071	0.47029	0.00674	0.06098	0.00054	441	17	391	5	382	3
29	592.1	8421.7	5251.0	0.62	0.05677	0.00179	0.46879	0.01247	0.05969	0.00077	482	36	390	9	374	5
30	197.9	2963.0	1606.6	0.54	0.05467	0.00091	0.46085	0.00760	0.06093	0.00038	399	26	385	5	381	2
31	306.5	4661.9	2156.9	0.46	0.05348	0.00079	0.45302	0.00654	0.06124	0.00039	349	21	379	5	383	2
32	148.4	2289.5	1016.2	0.44	0.05790	0.00117	0.48923	0.00997	0.06111	0.00040	526	33	404	7	382	2
33	163.7	2557.1	1029.8	0.40	0.05291	0.00095	0.44723	0.00801	0.06114	0.00037	325	30	375	6	383	2
34	330.7	5054.3	2485.6	0.49	0.05289	0.00053	0.44580	0.00434	0.06099	0.00036	324	12	374	3	382	2
35	151.3	2352.7	909.5	0.39	0.05137	0.00058	0.43606	0.00480	0.06146	0.00033	257	15	367	3	385	2
36	246.9	3971.5	1354.4	0.34	0.05210	0.00049	0.43946	0.00565	0.06105	0.00057	290	14	370	4	382	3
37	186.1	2933.6	1310.5	0.45	0.05445	0.00120	0.44986	0.00961	0.05992	0.00031	390	50	377	7	375	2
08QH-27 (East-Kouan pluton)																
1	55.1	831.2	570.6	0.69	0.05492	0.00077	0.44640	0.00638	0.05883	0.00033	409	22	375	4	369	2
2	61.8	907.6	691.6	0.76	0.05397	0.00073	0.43864	0.00613	0.05879	0.00032	370	22	369	4	368	2
3	36.4	548.4	348.8	0.64	0.05741	0.00105	0.46665	0.00905	0.05876	0.00034	507	32	389	6	368	2
4	20.3	312.0	166.9	0.53	0.05391	0.00102	0.43721	0.00805	0.05883	0.00040	367	29	368	6	369	2
5	41.0	617.7	403.1	0.65	0.05519	0.00083	0.44857	0.00744	0.05870	0.00039	420	25	376	5	368	2
6	50.6	736.1	588.6	0.80	0.05317	0.00081	0.43176	0.00671	0.05874	0.00035	336	24	364	5	368	2
7	17.8	279.9	160.2	0.57	0.05684	0.00160	0.46005	0.01356	0.05867	0.00066	485	45	384	9	368	4
8	52.8	772.5	563.8	0.73	0.05968	0.00104	0.48148	0.00953	0.05827	0.00056	592	26	399	7	365	3
9	43.7	680.5	371.1	0.55	0.05368	0.00075	0.43216	0.00615	0.05824	0.00033	357	22	365	4	365	2
10	42.2	622.1	445.4	0.72	0.05416	0.00080	0.44027	0.00685	0.05874	0.00035	378	24	370	5	368	2
11	9.2	141.3	76.4	0.54	0.05756	0.00237	0.46650	0.02028	0.05869	0.00081	513	71	389	14	368	5
12	36.9	566.5	325.2	0.57	0.05530	0.00094	0.44786	0.00788	0.05855	0.00038	424	28	376	6	367	2
13	30.8	474.6	267.9	0.56	0.05397	0.00102	0.43601	0.00912	0.05841	0.00057	370	30	367	6	366	3
14	35.0	516.4	340.8	0.66	0.05453	0.00152	0.44384	0.01226	0.05892	0.00042	393	49	373	9	369	3
15	29.7	436.2	287.0	0.66	0.05505	0.00104	0.44529	0.00886	0.05855	0.00050	414	29	374	6	367	3
16	25.6	377.0	267.8	0.71	0.05414	0.00107	0.43697	0.00870	0.05846	0.00038	377	33	368	6	366	2
17	71.5	1026.4	685.9	0.67	0.06574	0.00119	0.53188	0.01042	0.05848	0.00035	798	31	433	7	366	2
18	23.6	371.5	172.5	0.46	0.05402	0.00160	0.43328	0.01235	0.05817	0.00046	372	68	366	9	364	3
19	41.8	606.4	443.0	0.73	0.05287	0.00091	0.42953	0.00770	0.05879	0.00038	323	29	363	5	368	2
20	31.6	464.5	271.9	0.59	0.06063	0.00130	0.49098	0.01013	0.05878	0.00041	626	32	406	7	368	2
21	37.3	549.7	366.7	0.67	0.05435	0.00086	0.44103	0.00713	0.05876	0.00032	386	26	371	5	368	2
22	81.7	1152.3	972.7	0.84	0.05370	0.00078	0.43592	0.00635	0.05877	0.00029	359	24	367	4	368	2
23	21.3	293.4	215.3	0.73	0.06452	0.00221	0.52582	0.01799	0.05903	0.00049	759	58	429	12	370	3
24	27.9	418.7	259.8	0.62	0.05383	0.00141	0.43111	0.01182	0.05793	0.00047	364	47	364	8	363	3

(*continued on next page*)

Table 2 (*continued*)

Spot	Pb_{rad}	^{238}U (ppm)	^{232}Th (ppm)	Th/U	Isotopic ratios							Apparent age (Ma)					
					$^{207}Pb/^{206}Pb$	1σ	$^{207}Pb/^{235}U$	1σ	$^{206}Pb/^{238}U$	1σ		$^{207}Pb/^{206}Pb$	1σ	$^{207}Pb/^{235}U$	1σ	$^{206}Pb/^{238}U$	1σ
25	74.2	1035.0	879.7	0.85	0.05398	0.00087	0.43957	0.00735	0.05891	0.00039		370	26	370	5	369	2
26	63.4	903.7	707.5	0.78	0.05888	0.00138	0.47751	0.01154	0.05860	0.00034		563	43	396	8	367	2
27	27.4	408.6	260.3	0.64	0.05290	0.00103	0.42874	0.00857	0.05870	0.00051		324	30	362	6	368	3
28	41.6	468.5	326.5	0.70	0.05437	0.00645	0.43426	0.05082	0.05818	0.00075		386	241	366	36	365	5
29	49.2	724.5	491.0	0.68	0.05437	0.00089	0.43790	0.00711	0.05827	0.00033		386	26	369	5	365	2
30	46.3	633.6	606.6	0.96	0.05565	0.00099	0.44593	0.00743	0.05805	0.00030		438	28	374	5	364	2
31	54.8	792.0	494.8	0.62	0.05352	0.00115	0.43599	0.00897	0.05894	0.00037		351	35	367	6	369	2
32	10.1	145.1	104.6	0.72	0.05725	0.00200	0.46196	0.01572	0.05857	0.00052		501	59	386	11	367	3
33	38.9	555.0	366.4	0.66	0.05391	0.00172	0.43374	0.01316	0.05829	0.00051		367	53	366	9	365	3
34	33.0	498.0	269.2	0.54	0.05432	0.00125	0.44126	0.01098	0.05861	0.00047		384	41	371	8	367	3
35	45.8	648.5	483.7	0.75	0.05676	0.00119	0.46033	0.00991	0.05862	0.00034		482	37	384	7	367	2
36	29.5	445.4	256.5	0.58	0.05267	0.00203	0.42214	0.01692	0.05794	0.00073		315	68	358	12	363	4
37	38.1	562.4	334.0	0.59	0.05324	0.00108	0.43525	0.00889	0.05910	0.00031		339	37	367	6	370	2

5.3. Nd–Hf isotope compositions

The Kouan granites have high and positive $\varepsilon_{Nd}(t)$ values (+6.7 to +7.7) and one-stage depleted mantle Nd model ages (T_{DM}) of 543–617 Ma (Table 4; Fig. 8a). Compared with contemporary Altay arc granitoids, they exhibit higher $\varepsilon_{Nd}(t)$ and lower T_{DM} (Fig. 8a and b). Additionally, they have $\varepsilon_{Nd}(t)$ and T_{DM} values similar to those of contemporary (380–390 Ma) arc-related basaltic rocks (picrites, high-Ti basalts and boninites) from the southern Altay Range (Fig. 8a and b) (Niu et al., 2006; Zhang et al., 2009). The Qiakuerte granites have slightly lower $\varepsilon_{Nd}(t)$ values (+5.3 to +6.0) and older one-stage depleted mantle Nd model ages (575–665 Ma) (Table 4; Fig. 8a). They have $\varepsilon_{Nd}(t)$ and T_{DM} values similar to the contemporary Kalatongke ultramafic–mafic rocks (Li et al., 1998), which have been considered to be the products of mantle upwelling in a post-collisional setting (Chen and Jahn, 2004; Han et al., 2004) (Fig. 8b).

The West-Kouan granites (sample 08QH-25) have zircon $\varepsilon_{Hf}(t)$ values ranging from +11.0 to +14.1 (average +12.3) and T_{DM}(Hf) model ages ranging from 445 Ma to 583 Ma (average 524 Ma) (Table 5). The East-Kouan granites (sample 08QH-27) have zircon $\varepsilon_{Hf}(t)$ values ranging from +5.0 to +13.6 (average +11.3) (Table 5) and T_{DM}(Hf) model ages ranging from 455 to 845 Ma (average 555 Ma) (Table 5). The 382–367 Ma zircon granules from samples 08QH-25 and 08QH-27 have high $\varepsilon_{Hf}(t)$ values (+5.0 to +14.0). Zircon Hf isotope compositions of the West- and East-Kouan granites are slightly higher than those of the zircons from the Altay arc granitoids (Fig. 9a) (Sun et al., 2009).

The Saertielieke granites (sample 08WLG-16) have zircon $\varepsilon_{Hf}(t)$ values ranging from +11.6 to +18.7 (average +14.6) and T_{DM}(Hf) values ranging from 206 to 511 Ma (average 371 Ma) (Table 5). The Jierdekala granites (sample 08WLG-07) have zircon $\varepsilon_{Hf}(t)$ values ranging from +10.0 to +18.6 (average +12.5) and T_{DM}(Hf) ages ranging from 213 to 608 Ma (average 438 Ma) (Table 5). In summary, the Saertielieke and Jierdekala granites in the Qiakuerte area have high $\varepsilon_{Hf}(t)$ values close to the depleted mantle evolution line (Fig. 9a).

6. Discussion

6.1. Classification of the Kouan and Qiakuerte granites

Although the alkali mafic minerals arfvedsonite and aegirine (Fig. 3) occur in the Qiakuerte granites but are absent from the Kouan granites, both suites exhibit geochemical characteristics of A-type granites. These include high $Na_2O + K_2O$, FeO/MgO, Ga/Al and HFSE values, and low CaO, Sr, and Eu values (Figs. 5 and 7), exhibiting characteristics of A-type granites (Loiselle and Wones, 1979; Collins et al., 1982; Whalen et al., 1987; King et al., 1997; Bonin, 2007). On the Nb–Y-3 × Ga and Nb–Y–Ce triangular diagrams of Eby (1992), the Qiakuerte A-type granite samples plot in the A_2 field, and the Kouan A-type granite samples also plot in A_2 field, but near the boundary of A_1 and A_2 field (Fig. 10a and b). In the Ce/Nb–Y/Nb diagram (Eby, 1992), the Qiakuerte A-type granite samples plot near the IAB field, whereas the Kouan A-type granite samples near the boundary between the OIB and IAB fields (Fig. 10c).

6.2. Petrogenesis

A-type granites can form through several magmatic processes, including partial melting of crustal rocks (Model A), fractional crystallization of mantle-derived melts (Model B), AFC (crustal assimilation plus fractional crystallization) processes (Model C) and magma mixing between basaltic and crustal melts (Model D)

Table 3
Major oxides (wt%) and trace element (ppm) compositions of the A-type granites in the southern Altay Range.

Pluton sample	Saertielieke			Jierdekala	West-Kouan			East-Kouan	North-Kouan
	08WLG-13	08WLG-16	08WLG-17	08WLG-07	08QH-24	08QH-25	08QH-26	08QH-27	08QH-29
Major oxides									
SiO_2	73.88	73.94	74.44	77.43	76.88	75.43	69.40	74.52	73.20
TiO_2	0.21	0.27	0.30	0.14	0.08	0.09	0.41	0.17	0.29
Al_2O_3	14.22	13.20	12.80	11.34	12.37	12.76	15.11	13.38	13.70
Fe_2O_3	1.34	1.68	1.87	2.44	0.86	1.06	2.53	1.29	1.93
MnO	0.14	0.16	0.19	0.06	0.03	0.03	0.06	0.03	0.05
MgO	0.10	0.09	0.10	0.02	0.02	0.02	0.33	0.08	0.18
CaO	0.22	0.28	0.22	0.16	0.43	0.48	1.04	0.43	0.27
Na_2O	4.64	5.09	5.00	4.02	4.17	4.50	4.91	4.30	4.42
K_2O	4.90	4.89	4.79	4.10	4.80	5.12	5.38	5.46	5.53
P_2O_5	0.04	0.02	0.03	0.01	0.01	0.01	0.07	0.02	0.04
LOI	0.17	0.24	0.32	0.20	0.24	0.34	0.80	0.18	0.25
Total	99.88	99.86	100.07	99.91	99.89	99.85	100.03	99.86	99.85
Trace element									
Sc	3.54	3.20	4.48	4.37	0.96	1.03	6.38	2.98	3.70
Cr	0.27	0.30	0.73	0.74	0.19	0.19	0.16	0.53	0.72
Ni	0.74	0.22	0.94	0.03	0.09	0.11	0.07	0.85	0.39
Co	29.5	31.7	49.3	38.3	38.5	50.6	28.6	41.3	30.4
Ga	23.0	22.3	24.1	26.3	23.1	24.6	20.7	18.8	20.4
Ge	2.43	2.12	2.40	2.48	2.29	2.27	1.97	1.94	1.86
Rb	185	141	163	151	286	288	92.0	71.0	124
Sr	9.21	15.6	6.21	3.14	8.69	8.89	44.2	21.5	27.8
Y	49.6	30.3	37.9	80.8	49.3	62.1	43.6	23.8	46.0
Zr	567	360	442	1375	140	123	388	296	352
Nb	22.1	15.3	19.8	45.5	43.2	45.3	31.4	13.7	35.4
Ba	65.0	87.2	23.1	6.20	17.0	16.6	204	26.3	88.6
Hf	13.9	9.50	12.3	27.2	6.90	5.70	11.2	10.1	11.1
Ta	1.54	1.06	1.46	3.77	4.31	4.54	2.42	0.78	2.81
Th	21.1	11.4	14.5	16.1	27.0	24.7	6.80	3.10	9.00
U	5.68	2.81	3.39	4.17	5.20	4.45	2.22	1.37	2.34
La	34.9	46.1	59.8	61.2	29.4	27.2	43.1	23.2	35.1
Ce	83.3	93.7	136	137	65.7	64.8	83.0	50.0	74.9
Pr	10.3	11.6	15.1	17.2	8.63	8.22	9.68	6.29	9.26
Nd	38.7	41.6	54.4	62.3	31.7	30.8	35.2	24.4	33.5
Sm	8.07	7.36	9.64	12.9	7.78	7.46	6.88	4.75	6.83
Eu	0.62	0.54	0.55	0.18	0.09	0.10	0.61	0.11	0.28
Gd	7.31	5.94	7.45	11.4	7.25	7.46	6.55	4.15	5.94
Tb	1.37	0.99	1.26	2.37	1.52	1.62	1.25	0.79	1.25
Dy	8.56	5.63	7.39	14.8	9.72	10.4	7.88	4.70	8.01
Ho	1.84	1.16	1.47	3.23	1.99	2.29	1.68	1.00	1.84
Er	5.72	3.46	4.38	9.77	5.89	7.12	5.15	2.82	5.68
Tm	0.89	0.54	0.67	1.53	0.90	1.10	0.81	0.43	0.93
Yb	5.92	3.61	4.68	10.0	6.09	7.31	5.62	2.83	6.39
Lu	0.91	0.57	0.74	1.53	0.92	1.08	0.91	0.47	1.00
Rb/Sr	20.1	9.0	26.3	48.1	32.9	32.4	2.1	3.3	4.5
Rb/Ba	2.8	1.6	7.1	24.5	16.8	17.3	0.5	2.7	1.4
Eu/Eu^*	0.25	0.25	0.20	0.04	0.04	0.04	0.28	0.07	0.14

(Collins et al., 1982; Clemens et al., 1986; Whalen et al., 1987; Creaser et al., 1991; Eby, 1992; Turner et al., 1992; King et al., 1997; Wu et al., 2002; Yang et al., 2006; Dall'Agnol and de Oliveira, 2007; Wang et al., 2010).

6.2.1. Models B-D: fractional crystallization, AFC processes and magma mixing

Granitic magma can not be generated directly by mantle partial melting (Taylor and Mclennan, 1985), which can only produce mafic to intermediate magmas (Hofmann, 1988). Experimental studies also indicate that dry peridotites mostly generate mafic magma (e.g., Hirose and Kushiro, 1993; Baker et al., 1995), while hydrous peridotites can generate mafic to high-Mg andesitic magma (Hirose and Kawamoto, 1995; Hirose, 1997) by partial melting at varying pressures (0.5–3.0 GPa) and degrees (2–40%) of partial melting (Fig. 11a). Both the Qiakuerte and Kouan granites exhibit high SiO_2 (>69 wt%) but low MgO (<0.33 wt%) contents, suggesting they were not directly derived from the mantle (Fig. 11a).

Fractional crystallization of mantle-derived melts may be ruled out in the generation of the Qiakuerte granites based on the following evidence. The Qiakuerte granites are not directly associated with either contemporary mafic or intermediate igneous rocks, as would be expected if extensive fractional crystallization took place (Sylvester, 1989; Peccerillo et al., 2003; Shellnutt et al., 2009). Although they are coeval with the Kalatongke mafic–ultramafic complexes 50 km to the north of Qiakuerte town (Fig. 1), there is a compositional gap spanning 55 and 72 wt% SiO_2 between the mafic–ultramafic rocks and the A-type granites and the two suites do not display a continuous compositional trend (Appendix A), which is typical characteristic for fractional crystallization (e.g., Frost and Frost, 1997; Bogaerts et al., 2003; Kim et al., 2006). The older zircon core ages of ~330 Ma argue against the possibility that they were generated by fractional crystallization of mantle-derived melt. In addition, in the southern Altay Range, coeval and large-scale A-type granites (Late Carboniferous–Early Permian) are widely distributed, e.g., the Zhaheba-Armantai (Han et al., 1997) and Kalamaili A-type granites belt (Tang et al., 2007b; Mao et al., 2008b; Su et al., 2008), and they have characteristics similar to the Qiakuerte A-type granites with high SiO_2 (>70 wt%), low MgO (<0.2 wt%) contents and high $\varepsilon_{Nd}(t)$ (>+5) and $\varepsilon_{Hf}(t)$

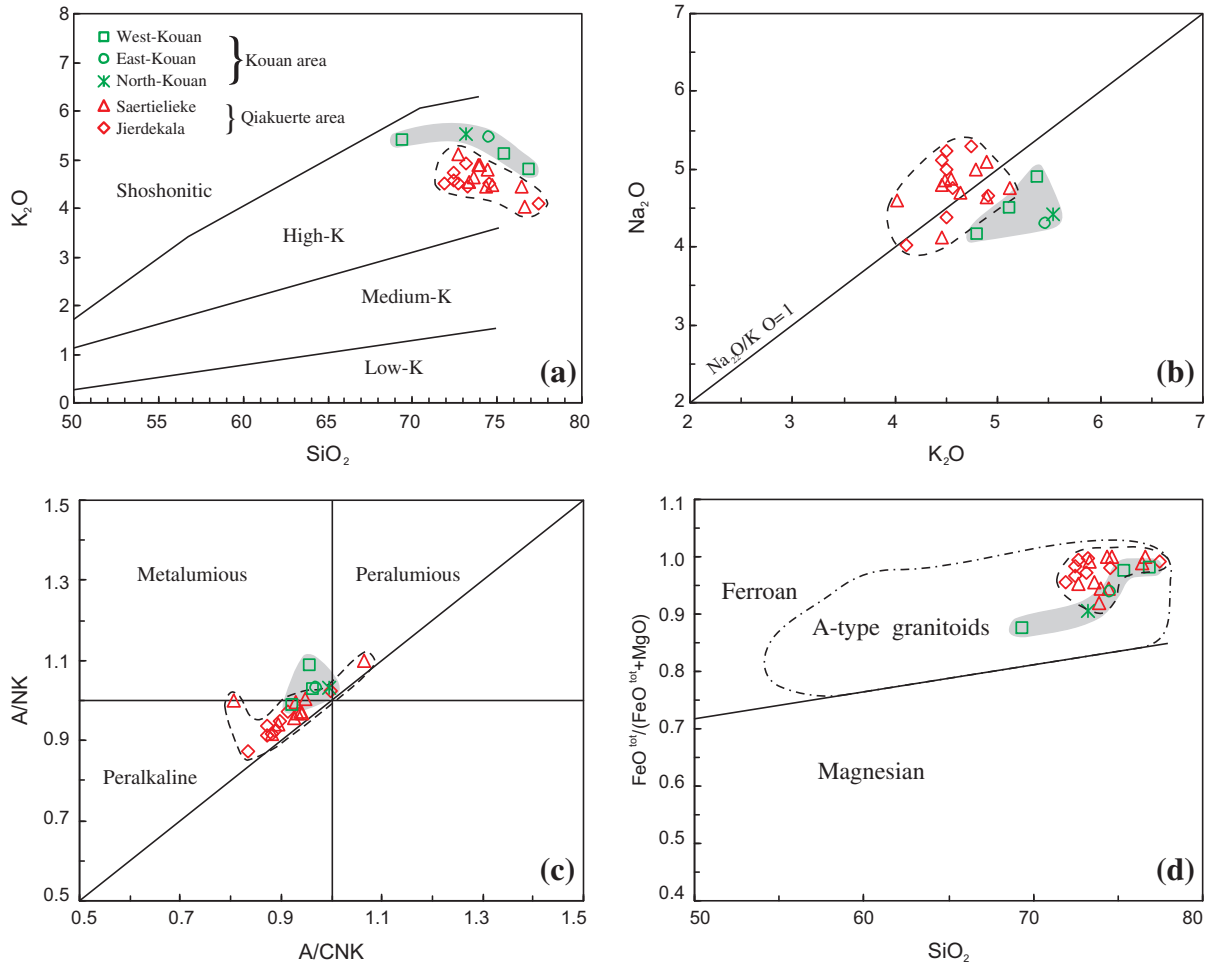

Fig. 5. Plots of (a) SiO_2 versus K_2O (Le Maitre et al., 1989); (b) Na_2O versus K_2O; (c) A/NK versus A/CNK; A/NK = $Al_2O_3/(Na_2O + K_2O)$, A/CNK = $Al_2O_3/(CaO + Na_2O + K_2O)$, molecular ratio; and (d) SiO_2 versus $FeO^{tot}/(FeO^{tot} + MgO)$ (Frost et al., 2001a) for the Qiakuerte and Kouan granites from the southern Altay Range. The data for the Qiakuerte granites are from Table 3 and Han et al. (1997).

(>+10) values (Han et al., 1997; Tang et al., 2007b, 2008; Mao et al., 2008b; Su et al., 2008). If such huge volumes of A-type granites were derived by extensive fractional crystallization of mantle melts, then the volume of mafic magma intruding into the crust may be an order of magnitude greater than that of A-type granites owing to the high degree of fractional crystallization (>90%) required by this model (Turner et al., 1992; Frost et al., 2002). However, coeval and spatially associated mafic rocks exposed in the southern Altay are very rare. Therefore, we suggest that fractional crystallization of mantle-derived mafic-intermediate magma is not a viable mechanism for the Qiakuerte A-type granites. However, their slightly variable SiO_2 contents (Fig. 8c) and Rb/Sr, Rb/Ba and Eu/Eu* ratios (Table 3) suggest that small degrees of fractional crystallization took place after the high silicate A-type granite magmas were generated.

Significant upper crust assimilation following generation of the Qiakuerte granitic magmas can also be discounted, based on their high and constant positive $\varepsilon_{Nd}(t)$ values that define a horizontal trend with increasing SiO_2 (Fig. 8c). Moreover, the Qiakuerte A-type granites have higher $\varepsilon_{Nd}(t)$ and $\varepsilon_{Hf}(t)$ and lower T_{DM}(Nd) values than those of contemporary granitoids in the Altay area, but partially overlap those of the contemporaneous Kalatongke mafic–ultramafic rocks (Fig. 8a and b), suggesting that crustal assimilation or magma mixing most likely did not play an important role in their petrogenesis.

Although the Kouan granite compositions extend to slightly lower silica contents (69 wt.% SiO_2) than the Qiakuerte granites, directly analogous arguments can be made against their petrogenesis via direct melting of the mantle (Fig. 11a) or by extensive crystal fractionation of mantle melts (Appendix B) (e.g., Zhang et al., 2007b). Minor variations in the SiO_2 contents (Fig. 8c) and Rb/Sr, Rb/Ba and Eu/Eu* ratios (Table 3) again suggest that small degrees of fractional crystallization did take place after the high silicate A-type granite magmas were generated. As is the case for the Qiakuerte granites, crustal assimilation or magma mixing were unlikely to have played an important role in the formation of the Kouan A-type granites. Their relatively high and uniform $\varepsilon_{Nd}(t)$ and $\varepsilon_{Hf}(t)$ and low T_{DM}(Nd) compared with contemporary calc-alkaline granitoids in the Altay area (Figs. 8 and 9), and similarity in isotopic compositions compared to contemporary basaltic volcanic rocks (Fig. 8a and b) argue against significant crustal input. A lack of inherited zircon (Fig. 4c and d) also suggests minimal addition of crustal components during the formation of the Kouan A-type granites. However, very minor assimilation of the middle-upper crust during magma ascent or partial melting of a mixed crustal source, consisting dominantly of new crustal material generated by underplated basaltic magmas with minor pre-existing potassium-rich lower crustal rocks (e.g., Wang et al., 2010), is possible, causing rare examples of zircons with relatively low $\varepsilon_{Hf}(t)$ values (+5.0 to +8.6) (Fig. 9a) and high whole-rock K_2O/Na_2O (1.1–1.3) ratios (Fig. 5b).

6.2.2. Model A: partial melting of juvenile basaltic crust

Partial melting in the stability field of plagioclase, as indicated by negative Eu, Ba and Sr anomalies of A-type granites, has been

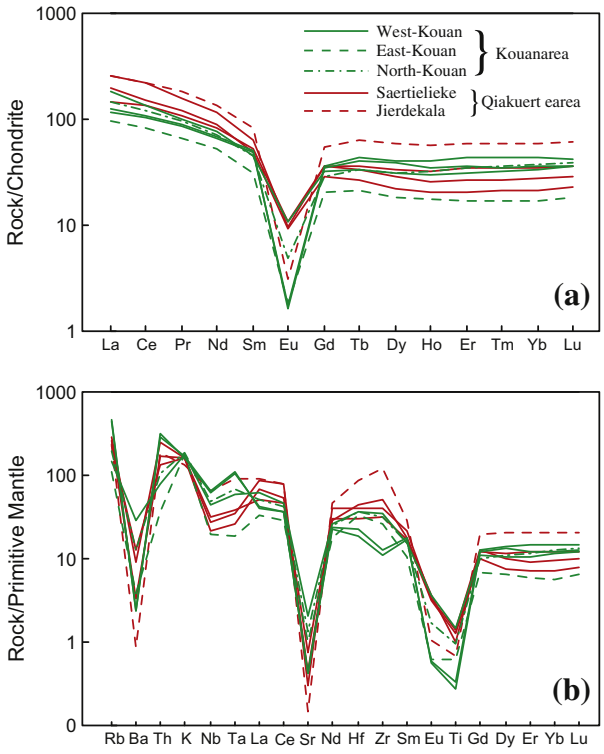

Fig. 6. Chondrite-normalized REE patterns (a) and primitive-mantle normalized diagrams (b) for the Kouan and Qiakuerte granites. Normalizing values are from Sun and McDonough (1989).

considered as an important mechanism for their generation, although the source rocks in the proposed models vary (e.g., Wang et al., 2010). Possible source rocks include F- and Cl-enriched lower crustal granulite residue (Collins et al., 1982; Clemens et al., 1986; Whalen et al., 1987), tonalite and granodiorite at low pressures (4 kbar) and high temperatures (950 °C) (Patiño Douce, 1997), and lower crustal basaltic rocks (Frost and Frost, 1997; Frost et al., 1999, 2001b; Dall'Agnol and de Oliveira, 2007). Creaser et al. (1991) have shown that a residual granulitic source is unlikely to generate A-type granitic melts as it is too refractory. Moreover, the residual model cannot explain some geochemical characteristics (e.g., high $FeO^{tot}/(FeO^{tot} + MgO)$) of A-type granites (Creaser et al., 1991; Frost and Frost, 1997; Wang et al., 2010). Bonin (2007) argues that the tonalite and granodiorite-derived experimental melts of Patiño Douce (1997) have higher CaO and K/Na ratios than typical A-type granites and melting temperatures of 950 °C cannot be expected at such shallow depths (less than 4 kbar). In addition, the A-type granites in the southern Altay range have higher $\varepsilon_{Nd}(t)$ and $\varepsilon_{Hf}(t)$ values than other granitoids in the present study area (Figs. 8b and 9a), which seems to be inconsistent with this model.

The high positive $\varepsilon_{Nd}(t)$ (+5.3 to +7.7) and $\varepsilon_{Hf}(t)$ (+5.0 to +18.7) values of the A-type granites in the Kouan and Qiakuerte areas suggest that their sources contain a depleted mantle component (Figs. 8 and 9) that may have been similar to juvenile basaltic crust. This conclusion is further supported by their young Nd model ages ranging from 543 to 665 Ma (Table 4 and Fig. 8a). In order to model partial melting of basaltic crust, we selected a Late Paleozoic amphibolite sample from the Tarlang area of the southern Altay Range ($\varepsilon_{Nd}(t) = 6.6$) (Hu et al., 2000; Cai et al., 2007) as the source of the Kouan and Qiakuerte A-type granites. The chondrite-normalized REE pattern of the A-type granites can largely be reproduced by 12% batch melting of the Tarlang amphibolite, except for slightly lower relative HREE contents (Fig. 11b). This may suggest that the HREE and the HFSE (e.g., Nb, Ta and Zr) were enhanced by the excess alkalis and the volatile component (e.g., F and Cl, particularly F) in the late stage fluid (Collins et al., 1982; Whalen et al., 1987; Turner et al., 1992). In any case, the modeling demonstrates that A-type granites of the southern Altay Range were most plausibly derived by partial melting of basaltic crust, irrespective of whether or not the Tarlang area amphibolite precisely matches the precursor of either the Kouan or Qiakuerte granites.

In fact, differences in the Nd–Hf compositions and major and trace elements characteristics of the Kouan and Qiakuerte A-type granites suggest that they were derived from different basaltic rocks, based on the following evidence:

(1) The Kouan A-type granites exhibit high $\varepsilon_{Nd}(t)$ and young $T_{DM}(Nd)$ similar to those of approximately contemporary (390–380 Ma) arc-related mafic–ultramafic rocks (picrites, high-Ti basalts and boninites) in the southern Altay Range (Fig. 8a and b). The Qiakuerte A-type granites exhibit high $\varepsilon_{Nd}(t)$ and young $T_{DM}(Nd)$ close to those of contemporaneous (305–287) Kalatongke mafic–ultramafic rocks, but distinct from the earlier (390–340 Ma) arc-related mafic–ultramafic rocks (Fig. 8a and b).

(2) The Kouan A-type granites have higher LILEs (e.g., Rb, Sr) and Nb/La ratios but lower HFSEs (e.g., Zr, Hf) and LREE contents than the Qiakuerte A-type granites (Figs. 6 and 8d). In combination with the higher $\varepsilon_{Nd}(t)$ values exhibited by the Kouan granites compared to the Qiakuerte granites, these differences suggest that source of the former contained more depleted mantle-derived components than that of the latter (Fig. 8).

Therefore, we argue that the early Kouan A-type granites (382–367 Ma) were generated from arc-related juvenile basaltic crust derived from depleted mantle sources (e.g., boninites), whereas the late Qiakuerte A-type granites (308–291 Ma) most plausibly originated from underplated basaltic crust derived from comparatively enriched mantle.

6.2.3. Hf–Nd isotope decoupling in the Qiakuerte granites

As illustrated in Fig. 9b, the zircon $\varepsilon_{Hf}(t)$ values of the Qiakuerte granites deviate positively from the whole-rock $\varepsilon_{Nd}(t)$ values compared to the normal terrestrial arrays for mantle and crust Hf–Nd isotope evolution (Vervoort et al., 1999), suggesting a Hf–Nd isotope decoupling (Patchett et al., 1981; Schmitz et al., 2004). Because zircon is resistant to weathering and may survive multiple episodes of metamorphism, partial melting, and hydrothermal alteration (Rubatto and Hermann, 2003; Spandler et al., 2004), it is capable of preserving its primary magmatic Hf isotopic composition (Wu et al., 2006c). Thus, the retention of radiogenic Hf in igneous zircons during partial melting of juvenile crustal material may have caused the decoupling of zircon Hf and whole-rock Nd isotopes in the Qiakuerte granites (Patchett et al., 1981; Wu et al., 2006c). In other words, zircon retains the Hf isotope signature acquired during crystallization from an earlier magma, whereas the whole-rock Sm–Nd system was readily equilibrated with the new melt and hence gave lower $\varepsilon_{Nd}(t)$ values (Wu et al., 2006c). As a result, the granites have less radiogenic Nd isotope compositions than normal terrestrial rocks at a given zircon $\varepsilon_{Hf}(t)$, and the inherited zircons display high $\varepsilon_{Hf}(t)$ ratios above the Hf–Nd terrestrial array (Fig. 9b). This is also the reason that zircon Hf model ages of the Qiakuerte granites are significantly younger than the whole-rock Nd model ages (Tables 4 and 5).

Another implication of the isotopic data is that the protolith of the Qiakuerte granites must have been derived from a more depleted mantle source than suggested by the compositions of the plutons, given that their parental magmas incorporated some

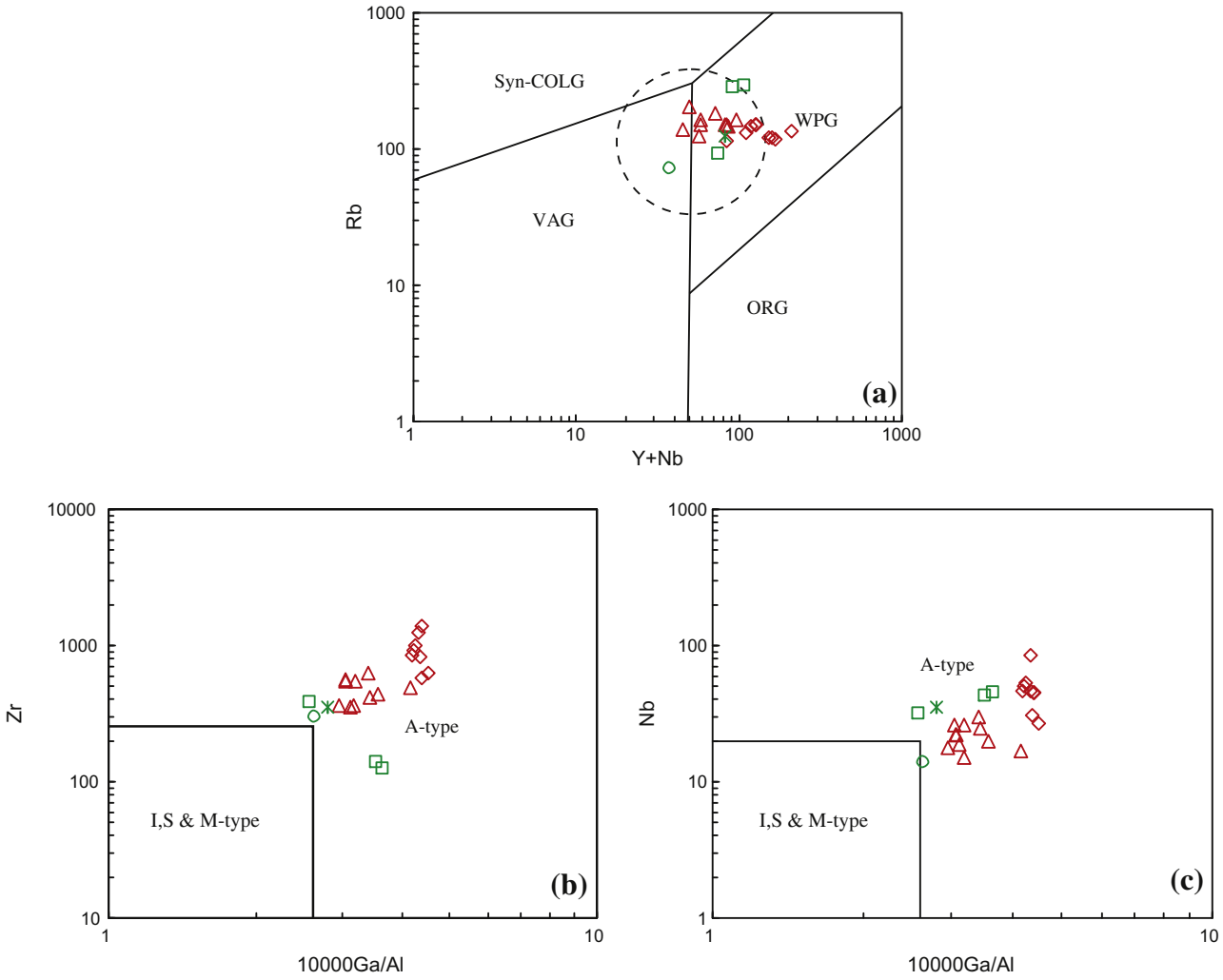

Fig. 7. (a) Tectonic discrimination diagram (Pearce, 1996). (b) Zr versus 10,000 Ga/Al discrimination diagram (Whalen et al., 1987) and (c) Nb versus 10,000 Ga/Al discrimination diagrams (Whalen et al., 1987) for granites. WPG = within plate granitoid, VAG = volcanic arc granitoid, Syn-COLG = syn-collision granitoid, ORG = ocean ridge granitoid. The data for the Qiakuerte granites are from Table 3 and Han et al. (1997). Symbols are the same as in Fig. 5.

Table 4
Nd isotope data of the A-type granites in the southern Altay Range.

Sample	Sm	Nd	$^{147}Sm/^{144}Nd$	$^{143}Nd/^{144}Nd$	2σ	$(^{143}Nd/^{144}Nd)_i$	$\varepsilon_{Nd}(t)$	T_{DM}	T_{2DM}
Qiakuerte area									
08WLG-13	8.07	38.72	0.1260	0.512769	8	0.512516	5.3	665	635
08WLG-16	7.36	41.60	0.1070	0.512749	7	0.512534	5.7	575	606
08WLG-17	9.64	54.37	0.1072	0.512746	7	0.512531	5.6	581	612
08WLG-07	12.90	62.29	0.1252	0.512809	6	0.512570	6.0	590	568
Kouan area									
08QH-24	7.782	31.72	0.1483	0.512911	7	0.512540	7.7	561	504
08QH-25	7.464	30.79	0.1466	0.512880	8	0.512513	7.2	617	547
08QH-26	6.879	35.24	0.1180	0.512795	8	0.512500	6.9	568	568
08QH-27	4.747	24.44	0.1174	0.512809	6	0.512527	7.1	543	544
08QH-29	6.831	33.45	0.1235	0.512797	7	0.512488	6.7	599	587

evolved crustal material at ca. 300 Ma. Partial melting caused newly grown zircon to have a lower $^{176}Hf/^{177}Hf$ ratio (Wu et al., 2006c), contrasting with a metamorphic effect that typically results in zircon overgrowths having higher $^{176}Hf/^{177}Hf$ ratios than associated cores (Zheng et al., 2005). Based on Fig. 9b, the dominant components of evolved crustal source for the Qiakuerte granites must have had a $\varepsilon_{Nd}(t)$ slightly lower than about +5 to +6 whereas the source of the inherited zircon cores had an $\varepsilon_{Nd}(t)$ near +8.

6.3. Tectonic setting and processes

Although both of the Kouan and Qiakuerte granites are geochemically similar to typical A_2-type granites, they differ in some key respects: (1) the Kouan plutons were emplaced in the Late Devonian (382–367 Ma), approximately synchronous with adakites, boninites, high-Ti basalts, picrites, ophiolites, and high temperature-low pressure metamorphic rocks, whereas the

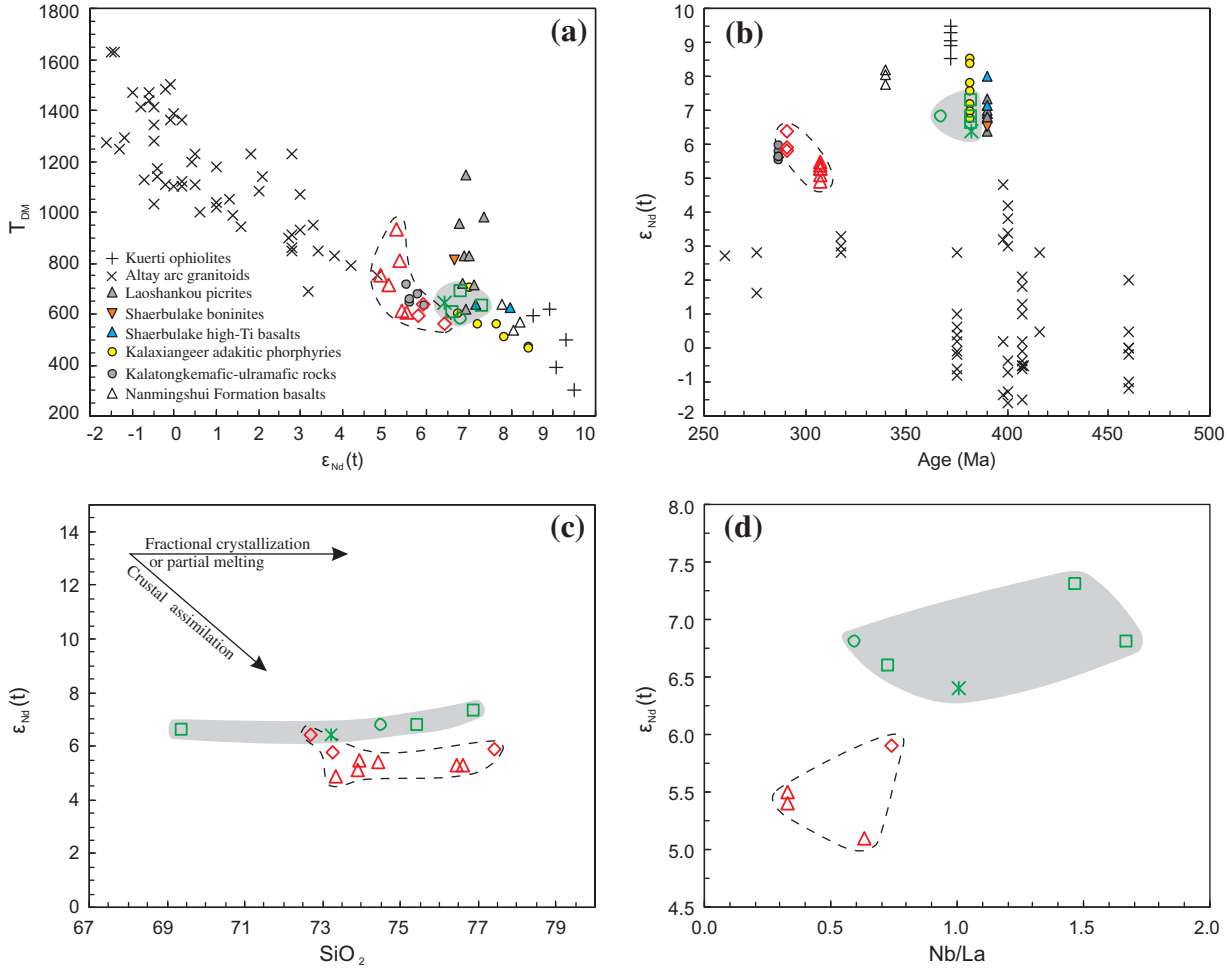

Fig. 8. (a) $\varepsilon_{Nd}(t)$ versus T_{DM} diagram. (b) $\varepsilon_{Nd}(t)$ versus age diagram. (c) SiO_2 versus $\varepsilon_{Nd}(t)$ diagram. (d) $\varepsilon_{Nd}(t)$ versus Nb/La diagram. Sources of data are the following: for Qiakuerte granites are from Table 4 and Han et al. (1997), for Altay arc granitoids are from Wang et al. (2009), for Kuerti ophiolites are from Xu et al. (2003), for Kalaxiangeer adakitic porphyries are from Wan and Zhang (2006) and Zhang et al. (2006), for Kalatongke mafic–ultramafic rocks are from Li et al. (1998), for Laoshankou picrites are from Zhang et al. (2008a), and for Shaerbulake boninites and high-Ti basalts are form Niu et al. (2006). Symbols are the same as in Fig. 5.

Qiakuerte plutons were emplaced in the Late Carboniferous–Early Permian (308–291 Ma), approximately coeval with some mafic–ultramafic rocks (Figs. 1b and 8a–b); (2) the Kouan plutons are slightly foliated (Fig. 3c), suggesting they were formed before or during orogenesis, whereas the Qiakuerte plutons are undeformed; (3) the Kouan A-type granites are mainly composed of alkali-feldspar granites, whereas the younger Qiakuerte A-type granites are mainly arfvedsonite and aegirine-bearing granites; (4) the Qiakuerte A-type granites plot in A_2 field; the Kouan A-type granites also plot in A_2 field, but near the boundary between the A_1 and A_2 fields (Fig. 10); (5) as suggested above, the Kouan and Qiakuerte A-type granites were probably generated from different sources. Collectively, these differences suggest that the Kouan and Qiakuerte A-type granites were generated in distinct tectonic environments: arc-related and post-collisional extensional settings, respectively.

6.3.1. Ridge subduction-related extension

As oceanic lithosphere subducts, the subduction zone will eventually interact with a spreading ridge (Delong and Fox, 1977; Sisson et al., 2003). Ridge subduction, therefore, is an integral component of the Wilson cycle (DeLong and Fox, 1977). When the spreading ridge descends into the mantle, spreading can continue for some time and form a "slab window" along the edges of the divergent slab (Dickinson and Snyder, 1979; Thorkelson, 1996). Upwelling of the asthenosphere through the slab window would produce anomalous thermal, physical and chemical effects in the surrounding asthenospheric mantle and lead to distinctive magmatic activity, metamorphism and sedimentation. Uplift of the hot asthenosphere will cause rifting of the overriding plate, which will then trigger formation of a series of fore-arc or back-arc basins (Bourgois et al., 1996; Sample and Reid, 2003). The thermal input of upwelling asthenosphere will cause partial melting of the slab edge, overlying mantle wedge and crustal rocks to produce adakites, Nb-enriched basalts, high-Mg rocks (boninites and picrites), tholeiites or chemically unusual ophiolites and A-type granites (Sisson et al., 2003; Martin et al., 2005; Mortimer et al., 2006; Escuder Viruete et al., 2007; Hung et al., 2007; Cole and Stewart, 2009; Tang et al., 2010b). In addition, the high temperature regime caused by asthenosphere upwelling may result in high- and/or low-grade metamorphism on the overriding plate (Brown, 1998; Iwamori, 2000).

Windley et al. (2007) were the first to suggest a ridge subduction model to account for the evolution of the Central Asian Orogenic Belt. They proposed that at least seven ridge subduction events occurred during the evolution of the CAOB. Some recent case studies have also supported ridge subduction in the CAOB (Jian et al., 2008; Geng et al., 2009; Tang et al., 2010b). Sun et al. (2009) also suggested that ridge subduction occured in the Altay Range at ~420 Ma based on Hf isotope evidence.

Table 5
Zircon Lu–Hf isotope data for the A-type granites in the southern Altay Range.

Spot	$^{176}Yb/^{177}Hf$	$^{176}Lu/^{177}Hf$	$^{176}Hf/^{177}Hf$	2σ	Age	$\varepsilon_{Hf}(t)$	2σ	T_{DM}
Sample 08WLG-16 (Saertielieke pluton)								
08WLG-16 01	0.149134	0.004877	0.282979	0.000032	307	13.1	1.1	431
08WLG-16 02	0.127240	0.004257	0.282999	0.000033	307	13.9	1.2	393
08WLG-16 03	0.095803	0.003367	0.282914	0.000033	333	11.6	1.2	511
08WLG-16 04	0.088590	0.003086	0.282954	0.000033	333	13.1	1.2	446
08WLG-16 05	0.144866	0.004806	0.283033	0.000038	307	15.0	1.3	345
08WLG-16 06	0.163442	0.005507	0.283069	0.000039	307	16.1	1.4	294
08WLG-16 07	0.116494	0.004029	0.283105	0.000038	307	17.7	1.3	225
08WLG-16 08	0.127104	0.004190	0.283118	0.000038	333	18.7	1.3	206
Sample 08WLG-07 (Jierdekala pluton)								
08WLG-07 01	0.044062	0.001307	0.283102	0.000075	327	18.6	2.7	213
08WLG-07 02	0.032691	0.000821	0.282992	0.000024	327	14.8	0.8	367
08WLG-07 03	0.323621	0.010464	0.282931	0.000033	291	10.0	1.2	608
08WLG-07 04	0.110319	0.002934	0.282874	0.000033	327	10.2	1.2	565
08WLG-07 05	0.019472	0.000501	0.282948	0.000023	291	12.5	0.8	425
08WLG-07 07	0.017351	0.000524	0.282926	0.000020	291	11.8	0.7	456
08WLG-07 08	0.026571	0.000805	0.282972	0.000025	291	13.3	0.9	395
Sample 08QH-25 (West-Kouan pluton)								
08QH-25 01	0.137513	0.004890	0.282946	0.000022	382	13.3	0.8	485
08QH-25 02	0.073789	0.002634	0.282909	0.000022	382	12.6	0.8	509
08QH-25 03	0.083961	0.003053	0.282886	0.000023	382	11.7	0.8	549
08QH-25 04	0.087756	0.003214	0.282957	0.000032	382	14.1	1.1	445
08QH-25 05	0.150048	0.005199	0.282888	0.000020	382	11.2	0.7	582
08QH-25 06	0.089977	0.003340	0.282909	0.000024	382	12.4	0.9	519
08QH-25 07	0.112956	0.003940	0.282898	0.000036	382	11.9	1.3	546
08QH-25 08	0.092605	0.003302	0.282899	0.000025	382	12.1	0.9	534
08QH-25 09	0.092934	0.003311	0.282912	0.000026	382	12.5	0.9	515
08QH-25 10	0.096638	0.003738	0.282933	0.000022	382	13.1	0.8	489
08QH-25 11	0.110948	0.003893	0.282872	0.000024	382	11.0	0.9	584
08QH-25 12	0.098998	0.003450	0.282914	0.000025	382	12.6	0.9	512
Sample 08QH-27 (East-Kouan pluton)								
08QH-27 01	0.093357	0.003438	0.282864	0.000027	367	10.5	1.0	589
08QH-27 02	0.132852	0.004860	0.282912	0.000028	367	11.8	1.0	538
08QH-27 03	0.095986	0.003531	0.282810	0.000029	367	8.6	1.0	672
08QH-27 04	0.089530	0.003298	0.282895	0.000022	367	11.6	0.8	539
08QH-27 05	0.084090	0.003059	0.282948	0.000025	367	13.6	0.9	456
08QH-27 06	0.124718	0.004500	0.282878	0.000026	367	10.8	0.9	584
08QH-27 07	0.074844	0.002769	0.282854	0.000030	367	10.3	1.0	592
08QH-27 08	0.135658	0.004922	0.282946	0.000026	367	13.1	0.9	484
08QH-27 09	0.034382	0.001308	0.282879	0.000025	367	11.6	0.9	534
08QH-27 10	0.136261	0.004988	0.282908	0.000027	367	11.7	0.9	545
08QH-27 11	0.142413	0.005197	0.282722	0.000036	367	5.0	1.3	846
08QH-27 12	0.111117	0.004072	0.282949	0.000027	367	13.4	1.0	468

^{176}Lu decay constant is 1.865×10^{-11}; T_{DM}, depleted mantle Hf model age.

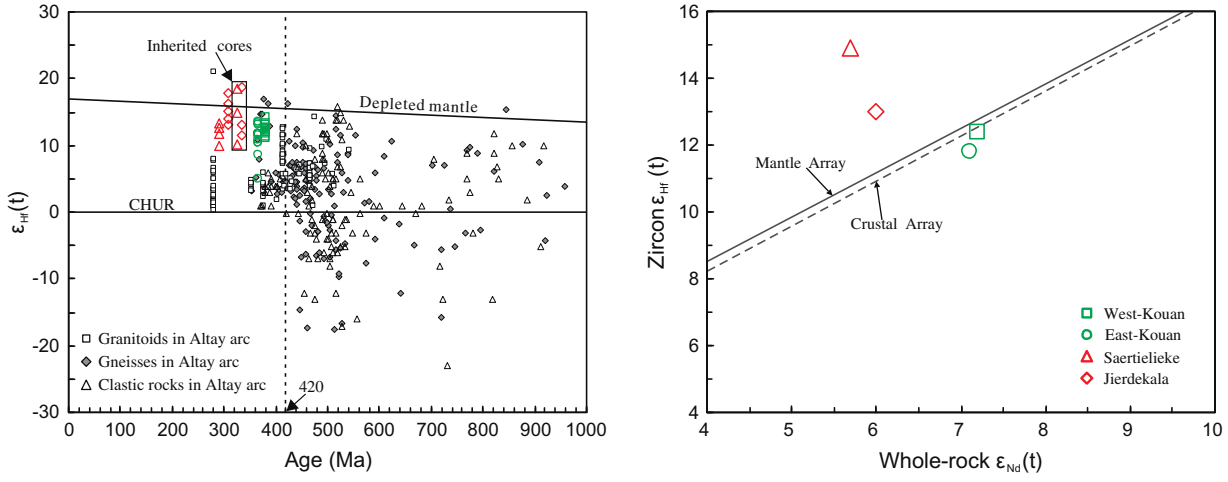

Fig. 9. (a) $\varepsilon_{Hf}(t)$-intrusive age diagram for the rocks of Kouan and Qiakuerte plutons. The data for the Altay arc granite are from Sun et al. (2009), those for the Altay arc gneiss are from Sun et al. (2008), and those for the Altay arc clastic rocks are from Long et al. (2007). Symbols are the same as in Fig. 5. (b) Zircon average $\varepsilon_{Hf}(t)$ versus whole-rock $\varepsilon_{Nd}(t)$ values for A-type granites in the southern Altay Range. Mantle and crust arrays are from Vervoort et al. (1999). Reference to the Mantle and Crustal Arrays suggest that the source rock of inherited zircons in the Qiakuerte plutons (Saertielieke and Jierdekala) had an $\varepsilon_{Nd}(t)$ value of about +8. Similarly, the $\varepsilon_{Nd}(t)$ of the evolved crustal source of these granites must have been slightly less than about +5 to +6, and probably comparable to the Kalatongke mafic–ultramafic suite.

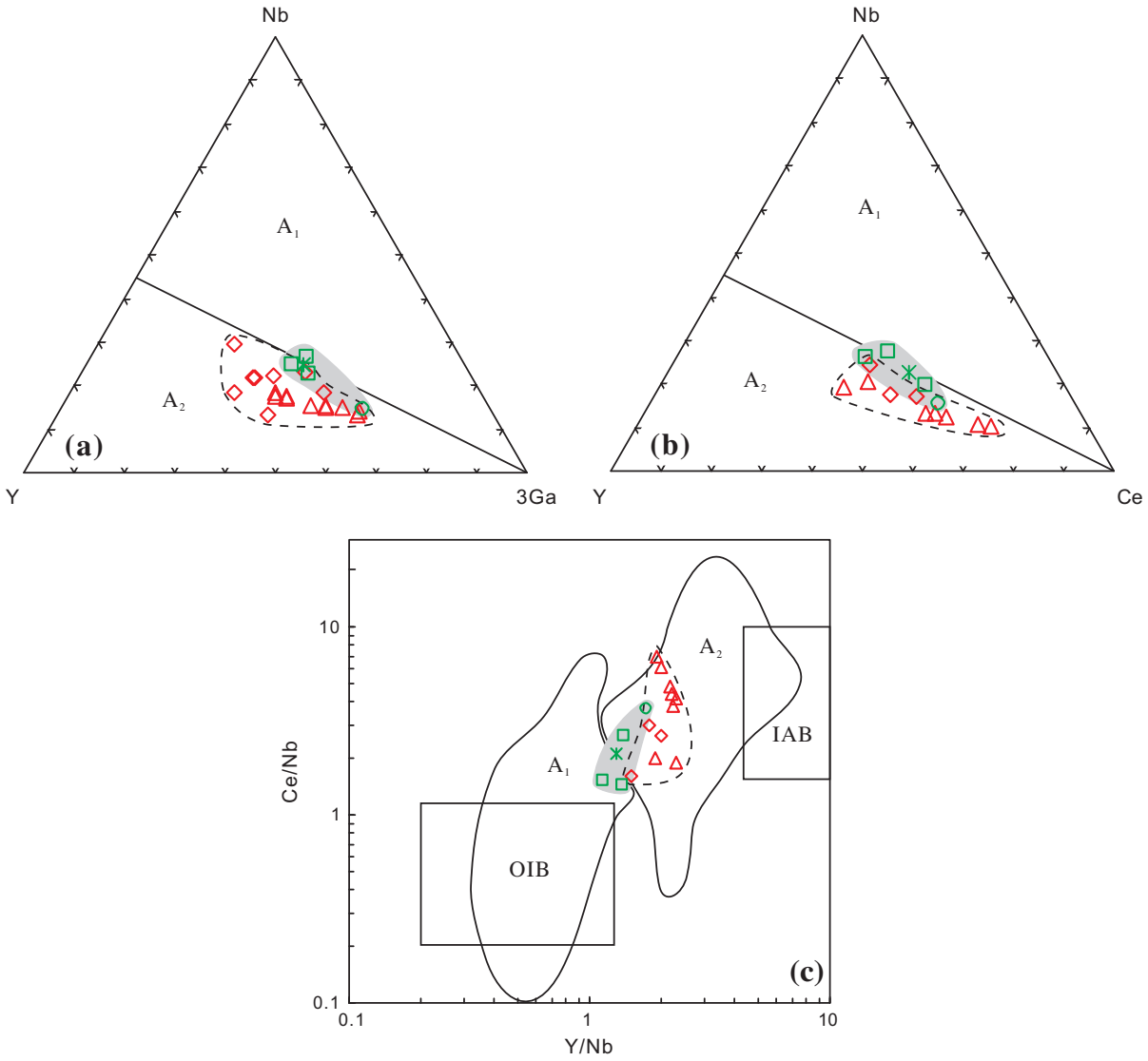

Fig. 10. Nb–Y–Ga (a) Nb–Y–Ce (b) and Ce/Nb–Y/Nb (c) discrimination diagrams for the subdivision of the A-type granites by Eby (1992). The data for the Qiakuerte granites are from Table 4 and Han et al. (1997). Symbols are the same as in Fig. 5.

A ridge subduction model can also account for an arc-related extensional setting for the Late Devonian (382–367 Ma) Kouan A-type granites in the southern Altay Range based on the following evidence: (1) Coeval (376–393 Ma) adakitic porphyries in the Kalaxiangeer porphyry copper belt (Figs. 1b and 12a) (Yang et al., 2005a; Wan and Zhang, 2006; Zhang et al., 2006; Xiang et al., 2009) exhibit MORB-like Nd–Sr isotope compositions ($\varepsilon_{Nd}(t)$ = +6.7 to +8.5, $(^{87}Sr/^{86}Sr)_i$ = 0.7037–0.7043) (Fig. 12b) and were most probably generated by the partial melting of slab edges in the subducting spreading ridge (e.g., Tang et al., 2010b); (2) Middle Devonian boninites in the Shaerbulake area about 20 km to the southwest of Fuyun City (Fig. 1b) were derived from depleted fore-arc mantle fluxed by slab-derived fluid (Zhang et al., 2003b; Niu et al., 2006) in response to the local injection of sub-slab asthenosphere; (3) Devonian high-Ti basalts in the Shaerbulake and Kuerti areas have the chemical characteristics of MORB (Niu et al., 2006) and may have been produced by the decompressional melting of upwelling asthenosphere; (4) Middle Devonian picrites in the Qiaoxiahala-Laoshankou area (Fig. 1b) exhibit arc-related geochemical features, suggesting that they were derived from mantle wedge (garnet-spinel transition zone) that was metasomatized by fluids released from altered oceanic crust (Zhang et al., 2008a); (5) Mafic rocks of the 372 ± 19 Ma Kuerti ophiolites display the compositional characteristics of both MORB and IAB (Xu et al., 2003; Zhang et al., 2003a), and basalts of 352 ± 4 Ma Qinghe ophiolites have the compositional characteristics of both IAB and OIB (Yang et al., 2005b; Wu et al., 2006a), including some Nb-enriched examples (Nb > 12.2 ppm) (Wu et al., 2006a). These compositionally diverse ophiolitic rocks are similar to basalts generated by ridge subduction, as documented in the Taitao peninsula (Lagabrielle et al., 1994) and Alaska (Bradley et al., 2003); (6) High-temperature and low pressure metamorphism took place at ~390 Ma in the Altay arc (Long et al., 2007; Wei et al., 2007), which is in agreement with a high temperature and low pressure regime caused by ridge subduction (Brown, 1998).

Age data suggest that there was an obvious gap (Gap 1) in the volume of typical calc-alkaline magmatism at ~400–380 Ma in the southern Altay Range (Fig. 13), which may reflect a decrease in fluid- induced metasomatism after the formation of the slab window (Thorkelson, 1996). This ridge subduction model is also supported by Hf isotope data in the Altay arc (Sun et al., 2009). Zircon Hf isotope compositions of the granitoids, gneisses, and

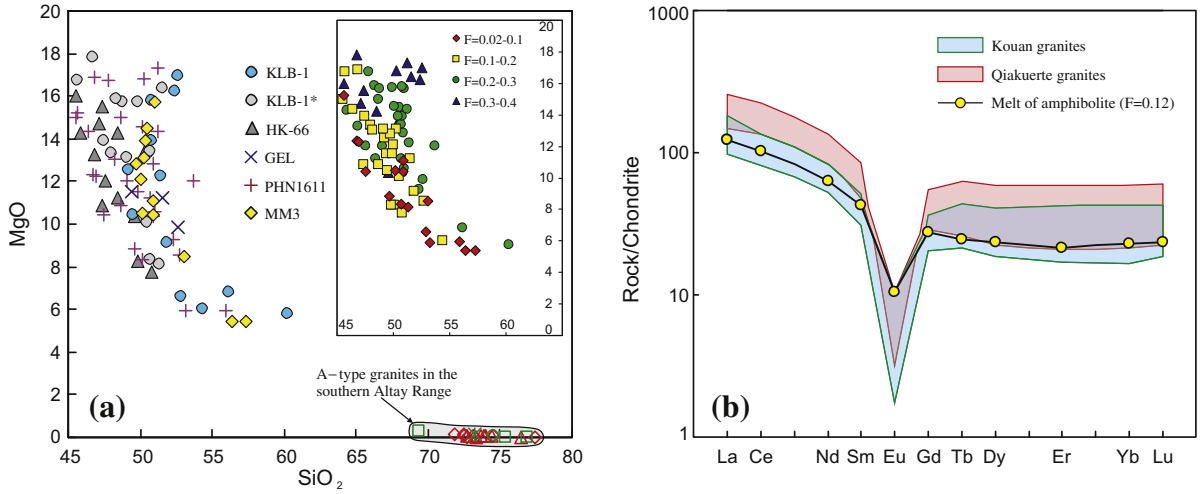

Fig. 11. (a) SiO_2–MgO diagram of the A-type granites in the southern Altay Range compared with the partial melts of peridotites at varying pressures (0.5–3 GPa). The peridotite-derived experimental melts (KLB-1) under hydrous condition are after Hirose and Kawamoto (1995) and Hirose (1997), and other experimental melts (KLB-1∗, HK-66, GEL, PHN1611 and MM3) in dry condition are after these references: Hirose and Kushiro (1993), Baker and Stolper (1994), Baker et al. (1995), Kushiro (1996) and Hirose and Kushiro (1998). F = degree of partial melting. (b) Model chondrite-normalized REE pattern compared with the A-type granites in the southern Altay Range. The REE pattern of the A-type granites is closely matched by the melt of amphibolite with 12% batch melting. The data for the Tarlang amphibolite in the southern Altay Range are from Cai et al. (2007). Bulk solid/melt partition coefficients of rhyolitic melts in equilibrium with an amphibolite residuum (35% Cpx, 45% Pl, and 20% Amph). Individual mineral K_d values are from Rollinson (1993) and references therein, and the Geochemical Earth Reference Model (GERM) (http://www.earthref.org).

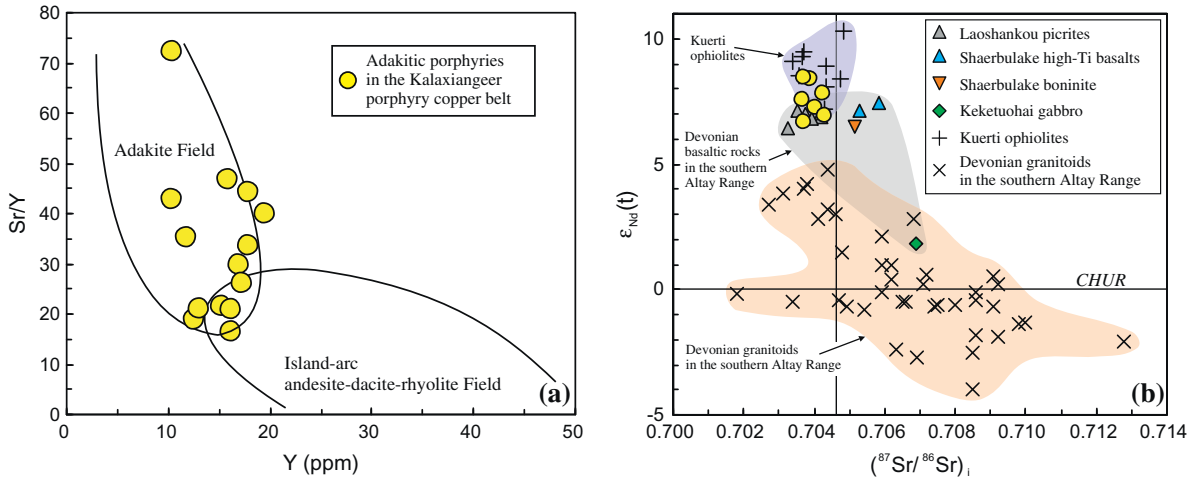

Fig. 12. (a) Sr/Y versus Y diagram (Defant and Drummond, 1993) for the Kalaxiangeer adakitic porphyries. (b) Nd and Sr isotope diagram for the Kalaxiangeer adakitic porphyries and Devonian igneous rocks in the southern Altay Range. The data for the Kalaxiangeer adakitic porphyries are from Yang et al. (2005a), Wan and Zhang (2006), and Zhang et al. (2006), the data for Keketuohai gabrro are from Wang et al. (2006), and the data for the Kuerti ophiolites, Shaerbulake high-Ti basalts and boninites, and Laoshankou picrites are from the same references as in Fig. 8.

sedimentary rocks in the Altay Range show an abrupt change at ~420 Ma (Fig. 9a), indicating that prior to that time the magmas came from both ancient and juvenile sources, whereas younger magmas were derived mainly from juvenile material (Sun et al., 2009). According to Sun et al. (2009), this dramatic change was due to the onset of ridge subduction in the Altay Range. Therefore, we suggest that ridge subduction was most likely responsible for the voluminous magmatism during the Devonian in the southern Altay Range. During ridge subduction, a slab window opened and the upwelling asthenosphere heated the lower juvenile crust, which may have been oceanic crust or newly underplated basaltic magma, resulting in the formation of the Kouan A_2-type granites. A similar process has been proposed for the Cretaceous Chatham Rise A-type granites, which are considered to have formed over a slab window during the subduction of the West Wishbone Ridge beneath eastern Zealandia (Mortimer et al., 2006). Numerous other occurrences of A-type granites generated in subduction-related extensional environments have been identified in recent years (Wu et al., 2002; Mortimer et al., 2006; Zhao et al., 2008; Chen et al., 2009; Ling et al., 2009; Wong et al., 2009), and these were triggered by oblique subduction, slab break-off, slab rollback, and ridge subduction.

6.3.2. Post-collisional extension

To date, the Late Carboniferous–Early Permian geodynamic setting of the southern Altay Range has remained controversial. Two distinctly different interpretations, arc (Han et al., 2006b; Long et al., 2006; Xiao et al., 2006, 2008, 2009) or post-collisional (Li, 2004; Han et al., 2006a; Wang and Xu, 2006; Zhang et al., 2009) settings, have been proposed. An arc setting, however, is not supported by several lines of geological evidence. Sedimentological studies indicated a Late Carboniferous–Permian continental volcanic-sedimentary sequence abruptly overlapped the earlier Paleozoic marine facies deposits in the southern Altay Range,

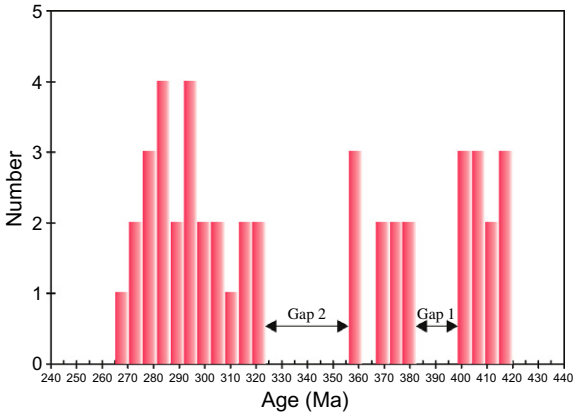

Fig. 13. Histogram of the zircon U–Pb ages for the southern Altay granite plutons. The ages are from Han et al. (2006a), Tong et al. (2006), Yuan et al. (2007), Sun et al. (2008), Wang et al. (2009), Xiang et al. (2009), and references therein.

suggesting a collisional event in the Carboniferous (Zhou et al., 2006; Zhang et al., 2008a, 2009). In addition, there are no deformed textures in the granitic plutons emplaced in the Late Carboniferous–Early Permian in the southern Altay Range (Fig. 3a) (Han et al., 1997; Chen and Jahn, 2004).

Alternatively, we suggest the southern Altay Range was in a post-collisional setting during the Late Carboniferous–Early Permian. The timing of oceanic crust subduction, ophiolite emplacement, and concomitant deformation and metamorphism most plausibly represent a pre-collisional stage through to the main collision period, implying that the sedimentary successions that unconformably overlie the deformed and metamorphosed lithologies correspond to the onset of a post-collisional setting (Liégeois, 1998; Wang and Xu, 2006). Li (2004) also suggested a post-collision stage in the Late Carboniferous for the southern Altay Range based on strata distribution, composition and their relationships with the ophiolites. Large-scale magmatic rocks (e.g., granitoids and Cu and Ni bearing mafic–ultramafic rocks) emplaced in the Late Carboniferous–Early Permian were broadly distributed in the southern Altay Range (Fig. 1). Granitic plutons in the Zhaheba-Armantai alkali granite belt, including the Saertielieke, Jierdekala, Sawudegeer, and Tasigake intrusions have Rb–Sr whole-rock isochron ages of between 309 Ma and 292 Ma (Wang et al., 1994; Han et al., 1997). The Sabei alkali granite of the Kalamaili alkali granite belt was generated in the Late Carboniferous (~306 Ma) (Tang et al., 2007b), and the Dajiashan and Huangyangshan granites in the same belt were generated between ~284 Ma and 305 Ma, respectively (Mao et al., 2008b; Su et al., 2008). The Kalatongke Cu–Ni–(PGE) sulfide-bearing ultramafic–mafic intrusions were generated at 283–305 Ma (Han et al., 2004, 2006b; Zhang et al., 2008b), and are considered to have been generated in a post-collisional setting (Han et al., 1999; Mao et al., 2008a; Zhang et al., 2008b). Age data (Fig. 13) for the southern Altay Range granites may further support the above conclusion: there is an otherwise unexplained gap in plutonism between ~325 and ~355 Ma (Gap 2) that could be accounted for as a time interval corresponding to the main phase of collision.

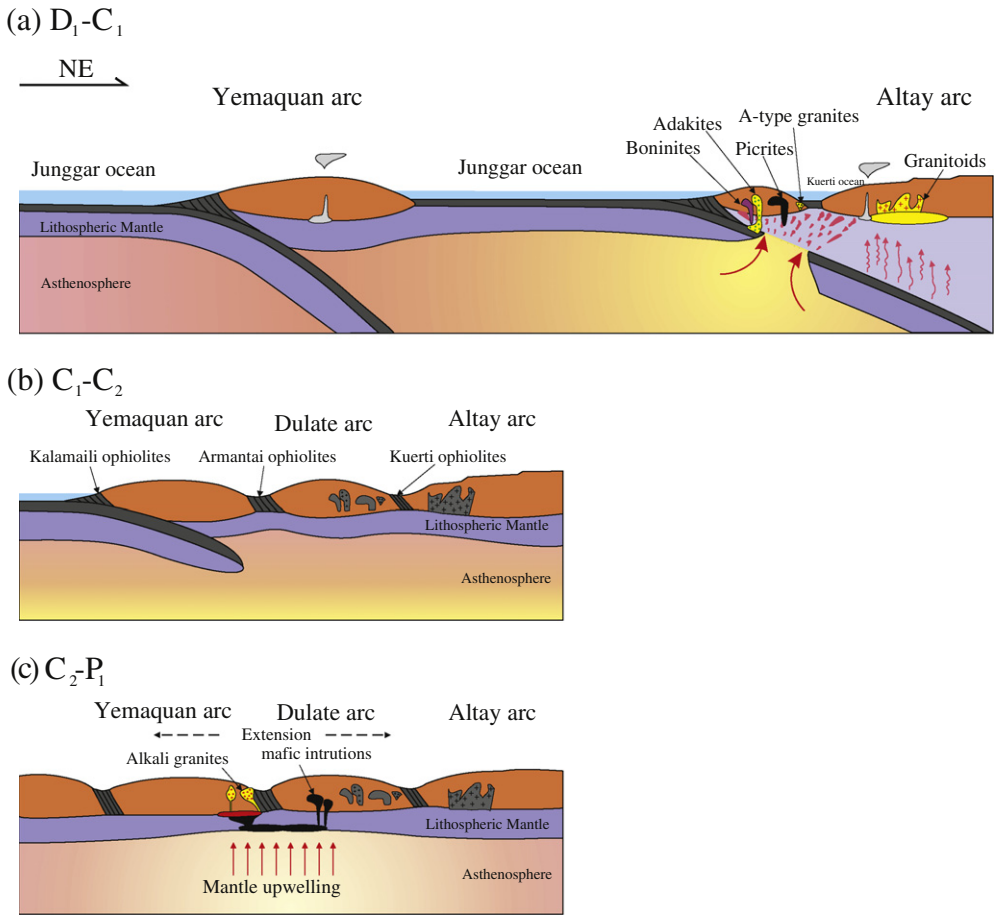

Fig. 14. Schematic diagrams showing a three-stage tectonic evolution of the Southern Altay Range (modified after Xiao et al., 2009; Zhang et al., 2009). (a) Devonian Subduction stage (D_1–C_1). (b) Early Carboniferous to Late Carboniferous Transformation stage (C_1–C_2). (c) Late Carboniferous to Early Permian Post-collision stage (C_2–P_1).

In summary, studies on the sedimentology, tectonics and magmatic rocks of the southern Altay Range collectively suggest that this area was in a post-collisional setting during the Late Carboniferous–Early Permian.

In a post-collisional setting, underplating basaltic magmas can provide heat for partial melting of crustal rocks (Ma et al., 1998; Mo et al., 2007; Zhao et al., 2009). Post-collisional or Late Carboniferous–Early Permian mafic–ultramafic intrusions in the southern Altay Range (e.g., the Kalatongke intrusions) indicate the occurrence of such underplating in the lower crust (Han et al., 1999). Therefore, we suggest that continued magma underplating led to partial melting of underplated juvenile lower crust to produce the A-type magmas in the Late Carboniferous–Early Permian (e.g., Wang et al., 2010). The Qiakuerte A-type granites have high $\varepsilon_{Nd}(t)$ values similar to those of coeval mafic–ultramafic intrusions (Fig. 8b), supporting such a conclusion.

6.3.3. Tectonic processes

Based on the above discussions and taking into consideration published data from northern Xinjiang (Xiao et al., 2008, 2009; Zhang et al., 2009), the Late Paleozoic tectonic evolution of the southern Altay Range can be divided into three stages. (1) Subduction stage (before 355 Ma, D_1–C_1): The ancient Junggar Ocean separated the Junggar Terrane and the Altay Terrane during the Devonian (He et al., 1994; Windley et al., 2002; Zhang et al., 2009) (Fig. 14a). Northward subduction eventually transported the spreading ridge to the subduction zone where ridge-trench interaction then occurred (DeLong and Fox, 1977). As a slab window opened, unusually high temperatures provided by the upwelling asthenosphere caused widespread melting of the subducted oceanic crust, mantle and overlying crust and generated corresponding metamorphism and widespread extension of the crust (Bourgois et al., 1996; Thorkelson, 1996; Brown, 1998; Sisson et al., 2003; Martin et al., 2005; Escuder Viruete et al., 2007). This sequence of events can account for the spectacular diversity of broadly coeval rocks found in the region, including adakites, boninites, high-Ti basalts, picrites, ophiolites and metamorphosed crustal rocks (Fig. 14a). Furthermore, the ridge subduction and upwelling asthenosphere also produced the Kouan A-type granites (Fig. 14a). (2) Transition stage from subduction to post-collision (355–308 Ma, C_1–C_2): Collision between the Junggar and the Altay terranes resulted in their amalgamation into a Cordilleran-type orogen (Goldfarb et al., 2003) at the end of the Early Carboniferous to the Late Carboniferous (Zhang et al., 2009) (Fig. 14b); (3) Post-collision stage (after 308 Ma, C_2–P_1): Voluminous A-type granites were generated and mafic–ultramafic intrusions were emplaced into the southern Altay Range (Fig. 14c). The generation of the post-collisional magmatism in the southern Altay Range was mainly triggered by the upwelling of the asthenospheric mantle in response to post-collisional detachment of the orogenic root zone (Han et al., 1999) or the ascent of a mantle plume (Zhou et al., 2004; Pirajno et al., 2008).

7. Conclusions

(1) Two episodes of A_2-type granite are identified in the southern Altay Range. The Kouan A-type granites were emplaced in Late Devonian (382–367 Ma) and the Qiakuerte A-type granites were emplaced in Late Carboniferous–Early Permian (308–291 Ma).

(2) The Late Devonian Kouan A-type granites are mainly composed of alkali-feldspar granites, and were probably derived from arc-related basaltic crust containing more depleted mantle-derived components. A ridge subduction model can account for the formation of the Kouan A_2-type granites.

(3) The late Qiakuerte A-type granites mainly consist of arfvedsonite and aegirine-bearing granites and most plausibly originated from re-melting of underplated basaltic lower crust with more enriched mantle-derived components. They were formed in a post-collision tectonic setting.

(4) A_2-type granites may not only form in post-collisional extensional settings, but also in ridge subduction-related extensional settings.

Acknowledgements

We sincerely thank Chief Editor Professor B.M. Jahn and two anonymous reviewers for their constructive and helpful reviews and Assistant Editor L. Jennifer for support with the review process. We also thank Professors Liu Yongsheng and Yang Jinhui, and Mr./Mrs. Liu Ying, Hu Guangqian, Ma Jinlong, Liang Xirong, Tu Xianglin and Zhang Hong for their assistance with laboratory work. This study was supported by research grants from the National Basic Research Program of China (2007CB411303), the Knowledge Innovation Program of Chinese Academy of Sciences (KZCX2-YW-128) and the National Natural Science Foundation of China (Grant No. 41025006). This is contribution No. IS-1265 from GIGCAS.

Appendix A. Supplementary material

Supplementary data associated with this article can be found, in the online version, at doi:10.1016/j.jseaes.2010.10.004.

References

Baker, M.B., Hirschmann, M.M., Ghiorso, M.S., Stolper, E.M., 1995. Compositions of near-solidus peridotite melts from experiments and thermodynamic calculations. Nature 375, 308–311.

Baker, M.B., Stolper, E.M., 1994. Determining the composition of high-pressure mantle melts using diamond aggregates. Geochimica et Cosmochimica Acta 58, 2811–2827.

Blichert-Toft, J., Albarède, F., 1997. The Lu–Hf isotope geochemistry of chondrites and the evolution of the mantle-crust system. Earth and Planetary Science Letters 148, 243–258.

Bogaerts, M., Scaillet, B., Liégeois, J.P., Vander Auwera, J., 2003. Petrology and geochemistry of the Lyngdal granodiorite (Southern Norway) and the role of fractional crystallisation in the genesis of Proterozoic ferro-potassic A-type granites. Precambrian Research 124, 149–184.

Bonin, B., 2007. A-type granites and related rocks: evolution of a concept, problems and prospects. Lithos 97, 1–29.

Bourgois, J., Martin, H., Lagabrielle, Y., Le Moigne, J., Jara, J.F., 1996. Subduction erosion related to spreading-ridge subduction: Taitao peninsula (Chile margin triple junction area). Geology 24, 723–726.

Bradley, D.C., Kusky, T.M., Haeussler, P.J., Goldfarb, R.J., Miller, M.L., Dumoulin, J.A., Nelson, S.W., Karl, S.M., 2003. Geologic signature of early Tertiary ridge subduction in Alaska. Geological Society of America 371, 19–49 (Special Paper).

Brown, M., 1998. Ridge-trench Interactions and High-T-low-P Metamorphism, with Particular Reference to the Cretaceous Evolution of the Japanese Islands. What Drives Metamorphism and Metamorphic Reactions? Geological Society, London, Special Publications 138, pp. 137–169.

Cai, K.D., Yuan, C., Sun, M., Xiao, W.J., Chen, H.L., Long, X.P., Zhao, Y.J., Li, J.L., 2007. Geochemical characteristics and ^{40}Ar–^{39}Ar ages of the amphibolites and gabbros in Tarlang area: implications for tectonic evolution of the Chinese Altai. Acta Petrologica Sinica 23, 877–888.

Charvet, J., Shu, L.S., Laurent-Charvet, S., 2007. Paleozoic structural and geodynamic evolution of eastern Tianshan (NW China); welding of the Tarim and Junggar plates. Episodes 30, 162–186.

Chen, B., Jahn, B.M., 2002. Geochemical and isotopic studies of the sedimentary and granitic rocks of the Altai orogen of northwest China and their tectonic implications. Geological Magazine 139, 1–13.

Chen, B., Jahn, B.M., 2004. Genesis of post-collisional granitoids and basement nature of the Junggar Terrane, NW China: Nd–Sr isotope and trace element evidence. Journal of Asian Earth Sciences 23, 691–703.

Chen, L., Ma, C.Q., She, Z.B., Mason, R., Zhang, J.Y., Zhang, C., 2009. Petrogenesis and tectonic implications of A-type granites in the Dabie orogenic belt, China: geochronological and geochemical constraints. Geological Magazine 146, 638–651.

Clemens, J.D., Holloway, J.R., White, A.J.R., 1986. Origin of an A-type granite; experimental constraints. American Mineralogist 71, 317–324.

Cole, R.B., Stewart, B.W., 2009. Continental margin volcanism at sites of spreading ridge subduction: examples from southern Alaska and western California. Tectonophysics 464, 118–136.
Collins, W.J., Beams, S.D., White, A.J.R., Chappell, B.W., 1982. Nature and origin of A-type granites with particular reference to southeastern Australia. Contributions to Mineralogy and Petrology 80, 189–200.
Creaser, R.A., Price, R.C., Wormald, R.J., 1991. A-type granites revisited: assessment of a residual-source model. Geology 19, 163–166.
Dall'Agnol, R., de Oliveira, D.C., 2007. Oxidized, magnetite-series, rapakivi-type granites of Carajas, Brazil: implications for classification and petrogenesis of A-type granites. Lithos 93, 215–233.
Defant, M.J., Drummond, M.S., 1993. Mount St. Helens: potential example of the partial melting of the subducted lithosphere in a volcanic arc. Geology 21, 547–550.
DeLong, S., Fox, P., 1977. Geological consequences of ridge subduction. In: Talwani, M., Pitman, W.C. (Eds.), Island Arcs, Deep Sea Trenches and Back-arc Basins. American Geophysical Union, Washington, DC, pp. 221–228.
Deng, J.H., Wang, D.Y., 1995. Characteristics and tectonic significance of ophiolite zones in Zaheba region, Fuyun County, Xinjiang. Journal of Chengdu University Technology 22, 8–14 (in Chinese with English abstract).
Dickinson, W.R., Snyder, W.S., 1979. Geometry of triple junctions related to San Andreas transform. Journal of Geophysical Research 84, 561–572.
Eby, G.N., 1992. Chemical subdivision of the A-type granitoids: petrogenetic and tectonic implications. Geology 20, 641–644.
Escuder Viruete, J., Contreras, F., Stein, G., Urien, P., Joubert, M., Pérez-Estaún, A., Friedman, R., Ullrich, T., 2007. Magmatic relationships and ages between adakites, magnesian andesites and Nb-enriched basalt-andesites from Hispaniola: record of a major change in the Caribbean island arc magma sources. Lithos 99, 151–177.
Frost, B.R., Barnes, C.G., Collins, W.J., Arculus, R.J., Ellis, D.J., Frost, C.D., 2001a. A geochemical classification for granitic rocks. Journal of Petrology 42, 2033–2048.
Frost, C.D., Frost, B.R., Bell, J.M., Chamberlain, K.R., 2002. The relationship between A-type granites and residual magmas from anorthosite: evidence from the northern Sherman batholith, Laramie Mountains, Wyoming, USA. Precambrian Research 119, 45–71.
Frost, C.D., Bell, J.M., Frost, B.R., Chamberlain, K.R., 2001b. Crustal growth by magmatic underplating: isotopic evidence from the northern Sherman batholith. Geology 29, 515–518.
Frost, C.D., Frost, B.R., Chamberlain, K.R., Edwards, B.R., 1999. Petrogenesis of the 1.43 Ga Sherman Batholith, SE Wyoming, USA; a reducted, rapakivi-type anorogenic granite. Journal of Petrology 40, 1771–1802.
Frost, C.D., Frost, B.R., 1997. Reduced rapakivi-type granites: the tholeiite connection. Geology 25, 647–650.
Geng, H.Y., Sun, M., Yuan, C., Xiao, W.J., Xian, W.S., Zhao, G.C., Zhang, L.F., Wong, K., Wu, F.Y., 2009. Geochemical, Sr–Nd and zircon U–Pb–Hf isotopic studies of Late Carboniferous magmatism in the West Junggar, Xinjiang: implications for ridge subduction? Chemical Geology 266, 373–398.
Goldfarb, R.J., Mao, J.W., Hart, C.J.R., Wang, D.H., Anderson, E.D., Wang, Z.L., 2003. Tectonic and metallogenic evolution of the Altay, northern Xinjiang Uygur Autonomous Region, northwestern China. In: Mao, J., Goldfarb, R.J., Seltmann, R. (Eds.). IAGOD Guidebook Series, London, pp. 17–30.
Griffin, W.L., Pearson, N.J., Belousova, E., Jackson, S.E., van Achterbergh, E., O'Reilly, S.Y., Shee, S.R., 2000. The Hf isotope composition of cratonic mantle; LA-MC-ICPMS analysis of zircon megacrysts in kimberlites. Geochimica et Cosmochimica Acta 64, 133–147.
Guo, F.F., Jiang, C.Y., Su, C.Q., Xia, M.Z., Xia, Z.D., Wei, W., 2008. Tectonic settings of A-type granites of Shaerdelan area, southeastern margin of Junggar block, Xinjiang, western China. Acta Petrologica Sinica 24, 2778–2788 (in Chinese with English abstract).
Han, B.F., He, G.Q., Wang, S.G., 1999. Post-collision mantle derived magmatism, underplating and the basement of Junggar basin. Science in China (Series D) 29, 16–21 (in Chinese).
Han, B.F., Ji, J.Q., Song, B., Chen, L.H., Li, Z., 2004. SHRIMP zircon U–Pb ages of Kalatongke No. 1 and Huangshandong Cu–Ni-bearing mafic–ultramafic complexes, North Xinjiang, and geological implications. Chinese Science Bulletin 49, 2324–2328 (in Chinese).
Han, B.F., Ji, J.Q., Song, B., Chen, L.H., Zhang, L., 2006a. Late Paleozoic vertical growth of continental crust around the Junggar Basin, Xinjiang, China (Part I): timing of post-collisional plutonism. Acta Petrologica Sinica 22, 1077–1086 (in Chinese with English abstract).
Han, B.F., Wang, S.G., Jahn, B.M., Hong, D.W., Kagami, H., Sun, Y.L., 1997. Depleted-mantle source for the Ulungur River A-type granites from North Xinjiang, China: geochemistry and Nd–Sr isotopic evidence, and implications for Phanerozoic crustal growth. Chemical Geology 138, 135–159.
Han, C.M., Xiao, W.J., Zhao, G.C., Qu, W.J., Mao, Q.G., Du, A.D., 2006b. Re–Os isotopic analysis of the Kalatongke Cu–Ni Sulfide Deposit, Northern Xinjiang, NW China, and its geological implication. Acta Petrologica Sinica 22, 163–170 (in Chinese with English abstract).
He, G.Q., Li, J.Y., Hao, J., Li, J.L., Cheng, S.D., Xu, X., XIao, X.C., Tian, P.R., Deng, Z.Q., Li, Y.A., Guo, F.X., 2001. Crustal structure and evolution of Xinjiang, China. In: C.N.P. 07-01 (Ed.), Urumqi, Xinjiang, China, pp. 227 (in Chinese with English abstract).
He, G.Q., Li, M.S., Liu, D.Q., Tang, Y.L., Zhou, R.H., 1994. Paleozoic Crust Evolution and Mineralization in Xingjiang of China. Xinjiang People's Publishing House, Urumqi. p. 437 (in Chinese with English abstract).
Hirose, K., 1997. Melting experiments on lherzolite KLB-1 under hydrous conditions and generation of high-magnesian andesitic melts. Geology 25, 42–44.
Hirose, K., Kawamoto, T., 1995. Hydrous partial melting of lherzolite at 1 GPa: the effect of H_2O on the genesis of basaltic magmas. Earth and Planetary Science Letters 133, 463–473.
Hirose, K., Kushiro, I., 1993. Partial melting of dry peridotites at high pressures: determination of compositions of melts segregated from peridotite using aggregates of diamond. Earth and Planetary Science Letters 114, 477–489.
Hirose, K., Kushiro, I., 1998. The effect of melt segregation on polybaric mantle melting: estimation from the incremental melting experiments. Physics of the Earth and Planetary Interiors 107, 111–118.
Hofmann, A.W., 1988. Chemical differentiation of the Earth: the relationship between mantle, continental crust, and oceanic crust. Earth and Planetary Science Letters 90, 297–314.
Hu, A.Q., Jahn, B.M., Zhang, G.X., Chen, Y.B., Zhang, Q.F., 2000. Crustal evolution and Phanerozoic crustal growth in northern Xinjiang: Nd isotopic evidence. Part I. Isotopic characterization of basement rocks. Tectonophysics 328, 15–51.
Hung, C., Chung, S., Cole, R., Iizuka, Y., Chiu, H., Chu, C., Gallet, S., Anonymous, 2007. Zircon U–Pb ages for the McKinley Sequence and Associated Plutons, Central Alaska Range. Eos, Transactions, American Geophysical Union 88 (Suppl. 52), 1–2.
Iwamori, H., 2000. Thermal effects of ridge subduction and its implications for the origin of granitic batholith and paired metamorphic belts. Earth and Planetary Science Letters 181, 131–144.
Jahn, B.M., Capdevila, R., Liu, D.Y., Vernon, A., Badarch, G., 2004. Sources of Phanerozoic granitoids in the transect Bayanhongor-Ulaan Baatar, Mongolia: geochemical and Nd isotopic evidence, and implications for Phanerozoic crustal growth. Journal of Asian Earth Sciences 23, 629–653.
Jahn, B.M., Wu, F.Y., Chen, B., 2000. Massive granitoid generation in Central Asia; Nd isotope evidence and implication for continental growth in the Phanerozoic. Episodes 23, 82–92.
Jian, P., Liu, D.Y., Kroer, A., Windley, B.F., Shi, Y.R., Zhang, F.Q., Shi, G.H., Miao, L.C., Zhang, W., Zhang, Q., Zhang, L.Q., Ren, J.S., 2008. Time scale of an early to mid-Paleozoic orogenic cycle of the long-lived Central Asian Orogenic Belt, Inner Mongolia of China: implications for continental growth. Lithos 101, 233–259.
Jian, P., Liu, D.Y., Zhang, Q., Zhang, F.Q., Shi, Y.R., Shi, G.H., Zhang, L.Q., Tao, H., 2003. SHRIMP dating of ophiolite and leucocratic rocks within ophiolite. Earth Science Frontiers 10, 439–456 (in Chinese with English abstract).
Kim, Sung W., Oh, Chang W., Ryu, I.C., Williams, I.S., Sajeev, K., Santosh, M., Rajesh, V.J., 2006. Neoproterozoic Bimodal volcanism in the Okcheon Belt, South Korea, and its comparison with the Nanhua Rift, South China: implications for Rifting in Rodinia. Journal of Geology 114, 717–733.
King, P.L., White, A.J.R., Chappell, B.W., Allen, C.M., 1997. Characterization and origin of aluminous A-type granites from the Lachlan fold belt, southeastern Australia. Journal of Petrology 38, 371–391.
Konopelko, D., Biske, G., Seltmann, R., Eklund, O., Belyatsky, B., 2007. Hercynian post-collisional A-type granites of the Kokshaal Range, Southern Tien Shan, Kyrgyzstan. Lithos 97, 140–160.
Kushiro, I., 1996. Partial melting of a fertile mantle peridotite at high pressures: an experimental study using aggregates of diamond. In: Basu, A.S., Hart, S. (Eds.), Earth Processes: Reading the Isotopic Code. Am. Geophys. Union, Geophys. Monogr. Ser. 95, pp. 109–122.
Lagabrielle, Y., Lemoigne, J., Maury, R.C., Cotten, J., Bourgois, J., 1994. Volcanic record of the subduction of an active spreading Ridge, Taitao Peninsula (Southern Chile). Geology 22, 515–518.
Le Maitre, R.W., Bateman, P., Dudek, A., Keller, J., Lameyre Le Bas, M.J., Sabine, P.A., Schmid, H., Streckeisen, A., Woolley, A.R., Zanettin, B., 1989. A Classification of Igenous Rocks and Glossary of Terms. Scientific Publications, Blackwell, Oxford. p. 193.
Li, H.Q., Xie, C.F., Chang, H.L., Cai, H., Zhu, J.P., Zhou, S., 1998. Study on Metallogenetic Charonology of Nonferrous and Precious Metallic ore Deposits in North Xinjiang, China. Geological Publishing House, Beijing. pp. 107–127, (in Chinese with English abstract).
Li, J.Y., 2004. Neoproterozoic and Paleozoic Tectonic Framework and Evolution of Eastern Xinjiang, NW China. Geological Review 50, 304–322 (in Chinese with English abstract).
Li, J.Y., Xiao, X.C., Tang, Y.Q., Zhao, M., Zhu, B.Q., Feng, Y.M., 1990. The main characteristics of Late Paleozoic plate tectonics in the southern part of East Junggar, Xinjiang. Chinese Geological Review 36, 305–316 (in Chinese with English abstract).
Li, X.H., Li, Z.X., Li, W.X., Liu, Y., Yuan, C., Wei, G.J., Qi, C.S., 2007. U–Pb zircon, geochemical and Sr–Nd–Hf isotopic constraints on age and origin of Jurassic I- and A-type granites from central Guangdong, SE China; a major igneous event in response to foundering of a subducted flat-slab? Lithos 96, 186–204.
Li, X.H., Li, Z.X., Wingate, M.T.D., Chung, S.L., Liu, Y., Lin, G.C., Li, W.X., 2006. Geochemistry of the 755 Ma Mundine Well dyke swarm, northwestern Australia: part of a Neoproterozoic mantle superplume beneath Rodinia? Precambrian Research 146, 1–15.
Li, X.H., Li, Z.X., Zhou, H.W., Liu, Y., Kinny, P.D., 2002. U–Pb zircon geochronology, geochemistry and Nd isotopic study of Neoproterozoic bimodal volcanic rocks in the Kangdian Rift of South China: implications for the initial rifting of Rodinia. Precambrian Research 113, 135–154.
Li, X.H., Qi, C.S., Liu, Y., Liang, X.R., Tu, X.L., Xie, L.W., Yang, Y.H., 2005. Petrogenesis of the Neoproterozoic bimodal volcanic rocks along the western margin of the Yangtze Block: newconstraints fromHf isotopes and Fe/Mn ratios. Chinese Science Bulletin 50, 2481–2486.

Liang, X.R., Wei, G.J., Li, X.H., Liu, Y., 2003. Precise determination of $^{143}Nd/^{144}Nd$ and Sm/Nd ratios using multiple-collector inductively coupled plasmamass spectrometer (MC-ICPMS). Geochimica 32, 91–96 (in Chinese with English abstract).
Liégeois, J.P., 1998. Preface – some words on the post-collisional magmatism. Lithos 45, 15–17.
Ling, M.X., Wang, F.Y., Ding, X., Hu, Y.H., Zhou, J.B., Zartman, R.E., Yang, X.Y., Sun, W.D., 2009. Cretaceous ridge subduction along the lower Yangze river belt, Eastern China. Economic Geology 104, 303–321.
Liu, J.Y., Yuan, K.R., 1996. A discussion on the genesis and tectonic setting of alkali granites in the Ulungur allali-rich granite belt, Xinjiang. Geological Journal of China University 2, 257–272 (in Chinese with English abstract).
Liu, W., 2002. Fluid–rock interaction during subsolidus microtextural development of alkali granite as exemplified by the Saertielieke pluton, Ulungur of the northern Xinjiang, China. Chemical Geology 182, 473–482.
Liu, W., Siebel, W., Li, X.J., Pan, X.F., 2005. Petrogenesis of the Linxi granitoids, northern Inner Mongolia of China: constraints on basaltic underplating. Chemical Geology 219, 5–35.
Liu, Y.S., Gao, S., Gao, C.G., Wang, D.B., Zong, K.Q., Hu, Z.C., 2010. Continental and oceanic crust recycling-induced melt-peridotite interactions in the Trans-North China Orogen: U–Pb dating, Hf isotopes and trace elements in zircons from mantle xenoliths. Journal of Petrology 51, 537–571.
Liu, Y.S., Hu, Z.C., Gao, S., Gunther, D., Xu, J., Gao, C.G., Chen, H.H., 2008. In situ analysis of major and trace elements of anhydrous minerals by LA-ICP-MS without applying an internal standard. Chemical Geology 257, 34–43.
Loiselle, M.C., Wones, D.R., 1979. Characteristics and origin of anorogenic granites. Geological Society of America Abstract with Programs 11, 468.
Long, X.P., Sun, M., Yuan, C., Xiao, W.J., Chen, H.L., Zhao, Y.J., Cai, K.D., Li, J.L., 2006. Genesis of Carboniferous volcanic rocks in the eastern Junggar: constraints on the closure of the Junggar Ocean. Acta Petrologica Sinica 22, 31–40 (in Chinese with English abstract).
Long, X.P., Sun, M., Yuan, C., Xiao, W.J., Lin, S.F., Wu, F.Y., Xia, X., Cai, K.D., 2007. Detrital zircon age and Hf isotopic studies for metasedimentary rocks from the Chinese Altai: implications for the Early Paleozoic tectonic evolution of the Central Asian Orogenic Belt. Tectonics 26 (TC5015). doi:10.1029/2007TC002128.
Ludwig, K.R., 2003. Isoplot 3.00: A Geochronological Toolkit for Microsoft Excel. Berkeley Geochronology Center, Berkeley, CA, USA.
Ma, C.Q., Li, Z.C., Ehlers, C., Yang, K.G., Wang, R.J., 1998. A post-collisional magmatic plumbing system: mesozoic granitoid plutons from the Dabieshan high-pressure and ultrahigh-pressure metamorphic zone, east-central China. Lithos 45, 431–456.
Mao, J.W., Pirajno, F., Zhang, Z.H., Chai, F.M., Wu, H., Chen, S.P., Cheng, L.S., Yang, J.M., Zhang, C.Q., 2008a. A review of the Cu–Ni sulphide deposits in the Chinese Tianshan and Altay orogens (Xinjiang Autonomous Region, NW China): principal characteristics and ore-forming processes. Journal of Asian Earth Sciences 32, 184–203.
Mao, Q.G., Xiao, W.J., Han, C.M., Yuan, C., Sun, M., 2008b. Late Paleozoic south-ward accretionary polarity of the eastern Junggar orogenic belt: insight from the Dajiashan and other A-type granites. Acta Petrologica Sinica 24, 733–742 (in Chinese with English abstract).
Martin, H., Smithies, R.H., Rapp, R., Moyen, J.F., Champion, D., 2005. An overview of adakite, tonalite–trondhjemite–granodiorite (TTG), and sanukitoid: relationships and some implications for crustal evolution. Lithos 79, 1–24.
Mo, X.X., Hou, Z.Q., Niu, Y.L., Dong, G.C., Qu, X.M., Zhao, Z.D., Yang, Z.M., 2007. Mantle contributions to crustal thickening during continental collision: evidence from Cenozoic igneous rocks in southern Tibet. Lithos 96, 225–242.
Mortimer, N., Hoernle, K., Hauff, F., Palin, J.M., Dunlap, W.J., Werner, R., Faure, K., 2006. New constraints on the age and evolution of the Wishbone Ridge, southwest Pacific Cretaceous microplates, and Zealandia-West Antarctica breakup. Geology 34, 185–188.
Niu, H.C., Sato, H., Zhang, H.X., Ito, J., Yu, X.Y., Nagao, T., Terada, K., Zhang, Q., 2006. Juxtaposition of adakite, boninite, high-TiO_2 and low-TiO_2 basalts in the Devonian southern Altay, Xinjiang, NW China. Journal of Asian Earth Sciences 28, 439–456.
Patchett, P.J., Kouvo, O., Hedge, C.E., Tatsumoto, M., 1981. Evolution of continental crust and mantle heterogeneity; evidence from Hf isotopes. Contributions to Mineralogy and Petrology 78, 279–297.
Patiño Douce, A.E., 1997. Generation of metaluminous A-type granites by low-pressure melting of calc-alkaline granitoids. Geology 25, 743–746.
Pearce, J., 1996. Sources and settings of granitic rocks. Episodes 19, 120–125.
Peccerillo, A., Barberio, M.R., Yirgu, G., Ayalew, D., Barbieri, M., Wu, T.W., 2003. Relationships between mafic and peralkaline silicic magmatism in continental rift settings; a petrological, geochemical and isotopic study of the Gedemsa Volcano, central Ethiopian Rift. Journal of Petrology 44, 2003–2032.
Pirajno, F., Mao, J.W., Zhang, Z.C., Zhang, Z.H., Chai, F.M., 2008. The association of mafic–ultramafic intrusions and A-type magmatism in the Tian Shan and Altay orogens, NW China: implications for geodynamic evolution and potential for the discovery of new ore deposits. Journal of Asian Earth Sciences 32, 165–183.
Rollinson, H., 1993. Using Geochemical Data. Longman, London. pp. 108–111.
Rubatto, D., Hermann, J., 2003. Zircon formation during fluid circulation in eclogites (Monviso, Western Alps): implications for Zr and Hf budget in subduction zones. Geochimica et Cosmochimica Acta 67, 2173–2187.
Sample, J.C., Reid, M.R., 2003. Large-scale, latest Cretaceous uplift along the Northeast Pacific Rim; evidence from sediment volume, sandstone petrography, and Nd isotope signatures of the Kodiak Formation, Kodiak Islands, Alaska. Geological Society of America 371, 51–70 (Special Paper).
Scherer, E., Muenker, C., Mezger, K., 2001. Calibration of the lutetium–hafnium clock. Science 293, 683–687.
Schmitz, M.D., Vervoort, J.D., Bowring, S.A., Patchett, P.J., 2004. Decoupling of the Lu–Hf and Sm–Nd isotope systems during the evolution of granulitic lower crust beneath southern Africa. Geology 32, 405–408.
Sengör, A.M.C., Natal'in, B.A., Burtman, V.S., 1993. Evolution of the Altaid tectonic collage and Palaeozoic crustal growth in Eurasia. Nature 364, 299–307.
Shellnutt, J.G., Zhou, M.F., Zellmer, G.F., 2009. The role of Fe–Ti oxide crystallization in the formation of A-type granitoids with implications for the Daly gap: an example from the Permian Baima igneous complex, SW China. Chemical Geology 259, 204–217.
Sisson, V.B., Pavlis, T.L., Roeske, S.M., Thorkelson, D.J., 2003. Introduction: an overview of ridge-trench interactions in modern and ancient settings. In: Sisson, V.B., Roeske, S.M., Pavlis, T.L. (Eds.), Geology of a Transpressional Orogen Developed during Ridge-trench Interaction along the North Pacific Margin. Geological Society of America (GSA), Boulder, CO, pp. 1–18.
Spandler, C., Hermann, J., Rubatto, D., 2004. Exsolution of thortveitite, yttrialite, and xenotime during low-temperature recrystallization of zircon from New Caledonia, and their significance for trace element incorporation in zircon. American Mineralogist 89, 1795–1806.
Su, Y.P., Tang, H.F., Hou, G.S., Liu, C.Q., 2006. Geochemistry of aluminous A-type granites along Darabut tectonic belt in West Junggar, Xinjian. Geochimica 35, 55–67 (in Chinese with English abstract).
Su, Y.P., Tang, H.F., Cong, F., 2008. Zircon U–Pb age and petrogenesis of the Huangyangshan alkaline granite body in the East Juggar, Xinjiang. Acta Mineralogica Sinica 28, 117–126.
Sun, M., Long, X.P., Cai, K.D., Jiang, Y.D., Wang, B.Y., Yuan, C., Zhao, G.C., Xiao, W.J., Wu, F.Y., 2009. Early Paleozoic ridge subduction in the Chinese Altai: insight from the abrupt change in zircon Hf isotopic compositions. Science in China Series D: Earth Sciences 52, 1345–1358.
Sun, M., Yuan, C., Xiao, W., Long, X., Xia, X., Zhao, G., Lin, S., Wu, F., Kroener, A., 2008. Zircon U–Pb and Hf isotopic study of gneissic rocks from the Chinese Altai; progressive accretionary history in the early to middle Palaeozoic. Chemical Geology 247, 352–383.
Sun, S.S., McDonough, W.F., 1989. Chemical and isotopic systematics of oceanic basalts: implications for mantle composition and processes. In: Saunder, A.D., Norry, M.J. (Eds.), Magmatism in the Ocean Basins. Geology Society Special Publication 42, 313–345.
Sylvester, P.J., 1989. Post-collisional alkaline granites. Journal of Geology 97, 261–280.
Tang, G.J., Wang, Q., Wyman, D.A., Sun, M., Li, Z.X., Zhao, Z.H., Sun, W.D., Jia, X.H., Jiang, Z.Q., 2010a. Geochronology and geochemistry of Late Paleozoic magmatic rocks in the Lamasu-Dabate area, northwestern Tianshan (west China): evidence for a tectonic transition from arc to post-collisional setting. Lithos 119, 393–411. doi:10.1016/j.lithos.2010.07.010.
Taylor, S.R., Mclennan, S.M., 1985. The Continental Crust: Its Composition and Evolution, an Examination of the Geochemical Record Preserved in Sedimentary Rocks. Blackwell Science Publisher, Oxford.
Tang, G.J., Wang, Q., Wyman, D.A., Li, Z.X., Zhao, Z.H., Jia, X.H., Jiang, Z.Q., 2010b. Ridge subduction and crustal growth in the Central Asian Orogenic Belt: evidence from Late Carboniferous adakites and high-Mg diorites in the western Junggar region, northern Xinjiang (west China). Chemical Geology 277, 281–300,. doi:10.1016/j.chemgeo.2010.08.012.
Tang, H.F., Qu, W.J., Su, Y.P., Hou, G.S., Du, A.D., Cong, F., 2007a. Genetic connection of Sareshike tin deposit with the alkaline A-type granites of Sabei body in Xinjiang: constraint from isotopic ages. Acta Petrologica Sinica 23, 1989–1997 (in Chinese with English abstract).
Tang, H.F., Su, Y.P., Liu, C.Q., Hou, G.S., Wang, Y.B., 2007b. Zircon U–Pb age of the Plagiogranite in Kalamaili belt, northern Xingjiang and its tectonic implications. Geotectonia et Metallogenia 31, 110–117 (in Chinese with English abstract).
Tang, H.F., Zhao, Z.Q., HUang, R.S., Han, Y.J., Su, Y.P., 2008. Primary Hf isotopic study on zircon from the A-type granites in eastern Junggar of Xinjiang, northwestern China. Acta Mineralogica Sinica 28, 335–342 (in Chinese with English abstract).
Thorkelson, D.J., 1996. Subduction of diverging plates and the principles of slab window formation. Tectonophysics 255, 47–63.
Tong, Y., Wang, T., Kovach, V.P., Hong, D.W., Han, B.F., 2006. Age and origin of the Takeshiken postorogenic alkali-rich intrusive rocks in southern Altai, near the Mongolian border in China and its implications for continental growth. Acta Petrologica Sinica 22, 1267–1278 (in Chinese with English abstract).
Turner, S.P., Foden, J.D., Morrison, R.S., 1992. Derivation of some A-type magmas by fractionation of basaltic magma: an example from the Padthaway Ridge, South Australia. Lithos 28, 151–179.
Vervoort, J.D., Patchett, P.J., Blichert-Toft, J., Albarède, F., 1999. Relationships between Lu–Hf and Sm–Nd isotopic systems in the global sedimentary system. Earth and Planetary Science Letters 168, 79–99.
Wan, B., Zhang, L.C., 2006. Geochemistry of ore-bearing porphyries in the Kalaxianger copper belt on the southeastern margin of the Altay Mountains, Xinjiang. Geology in China 33, 618–625 (in Chinese with English abstract).
Wang, J.B., Xu, X., 2006. Post-collisional tectonic evolution and metallogenesis in northern Xinjiang, China. Acta Geological Sinica 80, 23–31 (in Chinese with English abstract).
Wang, Q., Wyman, D.A., Li, Z.X., Bao, Z.W., Zhao, Z.H., Wang, Y.X., Jian, P., Yang, Y.H., Chen, L.L., 2010. Petrology, geochronology and geochemistry of ca. 780 Ma A-type granites in South China: petrogenesis and implications for crustal growth

during the breakup of supercontinent Rodinia. Precambrian Research 178, 185–208.
Wang, S.G., Han, B.F., Hong, D.W., Sun, Y.Y., 1994. Geochemistru and tectonic significance of alkali granites along Ulungur river, Xinjiang. Scientia Geologica Sinica 29, 373–383 (in Chinese with English abstract).
Wang, T., Hong, D.W., Jahn, B.M., Tong, Y., Wang, Y.B., Han, B.F., Wang, X.X., 2006. Timing, petrogenesis, and setting of Paleozoic synorogenic intrusions from the Altai Mountains, northwest China: implications for the Tectonic evolution of an accretionary orogen. Journal of Geology 114, 735–751.
Wang, T., Jahn, B.M., Kovach, V.P., Tong, Y., Hong, D.W., Han, B.F., 2009. Nd–Sr isotopic mapping of the Chinese Altai and implications for continental growth in the Central Asian Orogenic Belt. Lithos 110, 359–372.
Wei, C.J., Clarke, G., Tian, W., Qiu, L., 2007. Transition of metamorphic series from the Kyanite- to andalusite-types in the Altai orogen, Xinjiang, China: evidence from petrography and calculated KMnFMASH and KFMASH phase relations. Lithos 96, 353–374.
Whalen, J.B., Currie, K.L., Chappell, B.W., 1987. A-type granites: geochemical characteristics, discrimination and petrogenesis. Contributions to Mineralogy and Petrology 95, 407–419.
Windley, B.F., Alexeiev, D., Xiao, W.J., Kroner, A., Badarch, G., 2007. Tectonic models for accretion of the Central Asian Orogenic Belt. Journal of Geological Society, London 164, 31–47.
Windley, B.F., Kroener, A., Guo, J.H., Qu, G.S., Li, J.Y., Zhang, C., 2002. Neoproterozoic to Paleozoic geology of the Altai Orogen, NW China; new zircon age data and tectonic evolution. Journal of Geology 110, 719–737.
Wong, J., Sun, M., Xing, G., Li, X.H., Zhao, G.C., Wong, K., Yuan, C., Xia, X.P., Li, L.M., Wu, F.Y., 2009. Geochemical and zircon U–Pb and Hf isotopic study of the Baijuhuajian metaluminous A-type granite: extension at 125–100 Ma and its tectonic significance for South China. Lithos 112, 289–305.
Woodhead, J., Hergt, J., Shelley, M., Eggins, S., Kemp, R., 2004. Zircon Hf-isotope analysis with an excimer laser, depth profiling, ablation of complex geometries, and concomitant age estimation. Chemical Geology 209, 121–135.
Wu, B., He, G.Q., Wu, T.R., Li, H.J., Luo, H.L., 2006a. Discovery of the Buergen ophiolitic melange belt in Xinjiang and its tectonic significance. Geology in China 33, 476–486 (in Chinese with English abstract).
Wu, F.Y., Sun, D.Y., Li, H.M., Jahn, B.M., Wilde, S., 2002. A-type granites in northeastern China: age and geochemical constraints on their petrogenesis. Chemical Geology 187, 143–173.
Wu, F.Y., Yang, Y.H., Xie, L.W., Yang, J.H., Xu, P., 2006b. Hf isotopic compositions of the standard zircons and baddeleyites used in U–Pb geochronology. Chemical Geology 234, 105–126.
Wu, R.X., Zheng, Y.F., Wu, Y.B., Zhao, Z.F., Zhang, S.B., Liu, X., Wu, F.Y., 2006c. Reworking of juvenile crust: element and isotope evidence from Neoproterozoic granodiorite in South China. Precambrian Research 146, 179–212.
Wu, X.Q., Liu, D.L., Wei, G.Q., Li, J., Li, Z.S., 2009. Geochemical characteristics and tectonic settings of Carboniferous volcanic rocks from Ludong-Wucaiwan area, Junggar basin. Acta Petrologica Sinica 25, 55–66 (in Chinese with English abstract).
Xiang, P., Zhang, L.C., Wu, H.Y., Zhang, X.J., Chen, Z.G., Wan, B., 2009. Ages of the zircons from ore-bearing porphyries in II–III ore area of Kalaxianger porphyry copper ore belt in Qinghe, Xinjiang and its geological significance. Acta Petrologica Sinica 25, 1474–1483 (in Chinese with English abstract).
Xiao, W.J., Han, C.M., Yuan, C., Chen, H.L., Sun, M., Lin, S.F., Li, Z.L., Mao, Q.G., Zhang, J.E., Sun, S., Li, J.L., 2006. Unique Carboniferous–Permian tectonic–metallogenic framework of Northern Xinjiang (NW China): constraints for the tectonics of the southern Paieoasian Domain. Acta Petrologica Sinica 22, 1062–1076 (in Chinese with English abstract).
Xiao, W.J., Han, C.M., Yuan, C., Sun, M., Lin, S.F., Chen, H.L., Li, Z.L., Li, J.L., Sun, S., 2008. Middle Cambrian to Permian subduction-related accretionary orogenesis of Northern Xinjiang, NW China: implications for the tectonic evolution of central Asia. Journal of Asian Earth Sciences 32, 102–117.
Xiao, W.J., Windley, B.F., Yuan, C., 2009. Paleozoic mutiple subduction–accretion processes of the Southern Altaids. American Journal of Science 309, 221–270.
Xiao, X.C., Tang, Y.Q., 1991. Tectonic Evolution of the Southern Margin of the CENTRAL Asian Complex Megasuture Belt. Beijing Science and Technology Press, Beijing. pp. 6–25 (in Chinese with English abstract).
Xiao, X.C., Tang, Y.Q., Feng, Y.M., Zhu, B.Q., Li, J.Y., Zhao, M., 1992. Tectonic Evolution of the Northern Xinjiang and its Adjacent Regions. Geological Publishing House, Beijing. pp. 1–180 (in Chinese with English abstract).
Xu, J.F., Castillo, P.R., Chen, F.R., Niu, H.C., Yu, X.Y., Zhen, Z.P., 2003. Geochemistry of late Paleozoic mafic igneous rocks from the Kuerti area, Xinjiang, northwest China: implications for backarc mantle evolution. Chemical Geology 193, 137–154.
Yang, J.H., Wu, F.Y., Chung, S.L., Wilde, S.A., Chu, M.F., 2006. A hybrid origin for the Qianshan A-type granite, northeast China: geochemical and Sr–Nd–Hf isotopic evidence. Lithos 89, 89–106.
Yang, W.P., Zhang, Z.C., Zhou, G., Yang, S.H., He, L.X., Chen, B.L., 2005a. Discovery of the Xileketehalasu porphyry copper depisit on the southern margin of the Altay copper metallogenic belt. Geology in China 32, 107–114 (in Chinese with English abstract).
Yang, Z.H., Dong, L.H., Chen, M.Y., He, J.X., Hu, Z.J., Wang, B.Y., Song, J.F., Zhou, X.F., 2005b. New discovery of ophiolitic melange system in the Fuyun-Qinghe area in the Chinese Altay orogen. Earth Science Frontier 12, 177–178 (in Chinese).
Yuan, C., Sun, M., Xiao, W., Li, X., Chen, H., Lin, S., Xia, X., Long, X., 2007. Accretionary orogenesis of the Chinese Altai; insights from Paleozoic granitoids. Chemical Geology 242, 22–39.
Zhang, H.F., Parrish, R., Zhang, L., Xu, W.C., Yuan, H.L., Gao, S., Crowley, Q.G., 2007a. A-type granite and adakitic magmatism association in Songpan-Garze fold belt, eastern Tibetan Plateau: implication for lithospheric delamination. Lithos 97, 323–335.
Zhang, H.X., Niu, H.C., Sato, H., Yu, X.Y., Shan, Q., Zhang, B.Y., Ito, J., Nagao, T., 2005. Late Paleozoic adakites and Nb-enriched basalts from northern Xinjiang, northwest China; evidence for the southward subduction of the paleo-Asian oceanic plate. Island Arc 14, 55–68.
Zhang, H.X., Niu, H.C., Terada, K., Yu, X.Y., Sato, H., Ito, J., 2003a. Zircon SHRIMP U–Pb dating on plagiogranite from the Kuerti ophiolite in Altay, North Xinjiang. Chinese Science Bulletin 48, 1350–1354 (in Chinese).
Zhang, H.X., Niu, H.C., Yu, X.Y., Sato, H., Ito, J., Shan, Q., 2003b. Geochemical characteristics of the Shaerbulake boninites and their tectonic significance, Fuyun County, northern Xinjiang, China. Geochimica 32, 155–160 (in Chinese with English abstract).
Zhang, Q., Pan, G.Q., Li, C.D., Jin, W.J., Jia, X.Q., 2007b. Does fractional crystallization occur in granitic magma? Some crucial questions on granite study (2). Acta Petrologica Sinica 23, 1239–1251 (in Chinese with English abstract).
Zhang, Z.C., Mao, J.W., Cai, J., Kusky, T.M., Zhou, G., Yan, S., Zhao, L., 2008a. Geochemistry of picrites and associated lavas of a Devonian island arc in the northern Junggar terrane, Xinjiang (NW China): implications for petrogenesis, arc mantle sources and tectonic setting. Lithos 105, 379–395.
Zhang, Z.C., Yan, S.H., Chen, B.L., Zhou, G., He, Y.K., Chai, F.M., He, L.X., Wan, Y.S., 2006. SHRIMP zircon U–Pb dating for subduction-related granitic rocks in the northern part of east Junggar, Xinjiang. Chinese Science Bulletin 51, 952–962.
Zhang, Z.C., Zhou, G., Kusky, T.M., Yan, S.G., Chen, B.L., Zhao, L., 2009. Late Paleozoic volcanic record of the eastern Junggar Terrane, Xinjiang, northwestern China; major and trace element characteristics, Sr–Nd isotopic systematics and implications for tectonic evolution. Gondwana Research 16, 201–215.
Zhang, Z.H., Mao, J.W., Du, A.D., Pirajno, F., Wang, Z.L., Chai, F.M., Zhang, Z.C., Yang, J.M., 2008b. Re–Os dating of two Cu–Ni sulfide deposits in northern Xinjiang, NW China and its geological significance. Journal of Asian Earth Sciences 32, 204–217.
Zhao, X.F., Zhou, M.F., Li, J.W., Wu, F.Y., 2008. Association of Neoproterozoic A- and I-type granites in South China: implications for generation of A-type granites in a subduction-related environment. Chemical Geology 257, 1–15.
Zhao, Z.H., Wang, Z.G., Zou, T.R., Masuda, A., 1996. Study on petrogenesis of alkali-rich intrusive rocks of Ulungur, Xinjiang. Geochimica 25, 205–220 (in Chinese with English abstract).
Zhao, Z.H., Xiong, X.L., Wang, Q., Bai, Z.H., Qiao, Y.L., 2009. Late Paleozoic underplating in North Xinjiang: evidence from shoshonites and adakites. Gondwana Research 16, 216–226.
Zheng, Y.F., Wu, Y.B., Zhao, Z.F., Zhang, S.B., Xu, P., Wu, F.Y., 2005. Metamorphic effect on zircon Lu–Hf and U–Pb isotope systems in ultrahigh-pressure eclogite-facies metagranite and metabasite. Earth and Planetary Science Letters 240, 378–400.
Zhou, G., Zhang, Z.C., Gu, G.Z., Yang, W.P., He, B., Zhang, X.L., Luo, S.B., Wang, X., He, Y.K., 2006. Dating of granitic plutons and its geological implications in the lower reaches of the Qinggeli River in the northern part of East Junggar, Xinjiang. Geoscience 20, 141–150 (in Chinese with English Abstract).
Zhou, M.F., Michael, L.C., Yang, Z.X., Li, J.W., Sun, M., 2004. Geochemistry and petrogenesis of 270 Ma Ni–Cu–(PGE) sulfide-bearing mafic intrusions in the Huangshan district, Eastern Xinjiang, Northwest China: implications for the tectonic evolution of the Central Asian orogenic belt. Chemical Geology 209, 233–257.
Zhou, T.F., Yuan, F., Fan, Y., Zhang, D.Y., Cooke, D., Zhao, G.C., 2008. Granites in the Sawuer region of the west Junggar, Xinjiang Province, China: geochronological and geochemical characteristics and their geodynamic significance. Lithos 106, 191–206.